Cell Reports
Methods

Report

High-throughput histopathology for complex *in vitro* models

Graphical abstract

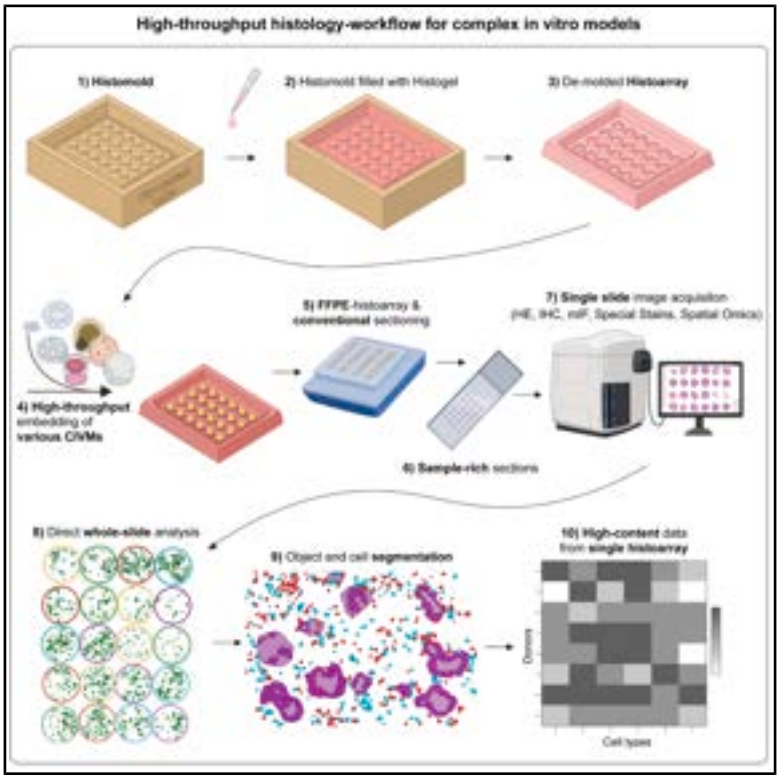

Highlights

- 3D-printed histomolds enable high-throughput co-planar embedding of CIVMs
- Up to 80 CIVM samples can be analyzed in a single histological section
- Model-specific molds support spatially controlled sectioning and downstream analysis
- This workflow reduces resource use, democratizing CIVM histopathology workflows

Authors

Marius F. Harter, Elisa D'Arcangelo, Julien Aubert, ..., Jose Luis Garcia-Cordero, Iago Pereiro, Nikolche Gjorevski

Correspondence

jose_luis.garcia_cordero@roche.com (J.L.G.-C.), pereiro@unistra.fr (I.P.), nikolche.gjorevski@roche.com (N.G.)

In brief

Harter et al. present 3D-printed histomolds that enable high-throughput embedding of various complex *in vitro* models (CIVMs) within a single FFPE block, providing high-content sections for spatial analysis. This resource-efficient workflow significantly lowers technical and cost hurdles, democratizing high-throughput embedding of CIVMs for histological assessment.

Harter et al., 2026, Cell Reports Methods *6*, 101419
June 15, 2026
https://doi.org/10.1016/j.crmeth.2026.101419

CellPress

Cell Reports Methods

CellPress
OPEN ACCESS

Report

High-throughput histopathology for complex *in vitro* models

Marius F. Harter,[1,2] Elisa D'Arcangelo,[1] Julien Aubert,[1] Barbora Lavickova,[1] Charles Havnar,[3] Bilgenaz Stoll,[1] Irineja Cubela,[1] Adrian M. Filip,[1] Laura Gaspa-Toneu,[1] Julian Scherer,[1] Evdoxia Karagkiozi,[4] Jean-Samuel Dupré,[1,5] Rubén López-Sandoval,[1,5] Rebecca Hsia,[6] Leah M. Norona,[7] Giovanna Brancati,[1,8] Ryo Okuda,[1] J. Gray Camp,[1,9] Eliah R. Shamir,[3] Jose Luis Garcia-Cordero,[1,*] Iago Pereiro,[1,*] and Nikolche Gjorevski[1,10,*]

[1]Institute of Human Biology (IHB), Roche Pharma Research and Early Development, Roche Innovation Center Basel, Basel, Switzerland
[2]Gustave Roussy Cancer Campus, University Paris-Saclay, Paris, France
[3]Department of Pathology, Genentech, Inc., South San Francisco, CA, USA
[4]Roche Innovation Center Basel, Roche Pharma Research and Early Development, Basel, Switzerland
[5]Department of Biosystems Science and Engineering, ETH Zurich, Basel, Switzerland
[6]Complex in vitro Systems Group, Genentech, Inc., South San Francisco, CA, USA
[7]Predictive Toxicology, Genentech, Inc., South San Francisco, CA, USA
[8]Immunology and Regenerative Medicine, Genentech, Inc., South San Francisco, CA, USA
[9]Biozentrum, University of Basel, Basel, Switzerland
[10]Lead contact
*Correspondence: jose_luis.garcia_cordero@roche.com (J.L.G.-C.), pereiro@unistra.fr (I.P.), nikolche.gjorevski@roche.com (N.G.)
https://doi.org/10.1016/j.crmeth.2026.101419

MOTIVATION Human complex *in vitro* models (CIVMs) have demonstrated remarkable potential to study tissue development, physiology, and disease at high throughput. To effectively employ these miniaturized systems in translational preclinical research, their in-depth benchmarking is pivotal. Histology has been the core of tissue characterization for centuries and the foundation of spatial phenotyping. However, standard histology workflows are inherently low throughput and centered on large tissue pieces. This does not match the high sample volumes and small sample sizes in CIVM research. To address this, we introduce 3D-printed histomolds and associated workflows that enables high-throughput embedding of CIVMs within a single FFPE block.

SUMMARY

Histology has been a cornerstone for complex *in vitro* model (CIVM) characterization for decades. However, it remains a low-throughput method with time-consuming workflows. Here, we introduce a holistic "histo-workflow," utilizing 3D-printed histomolds that facilitate co-planar embedding of CIVMs at high throughput, resulting in up to 80 samples in one section. We developed a variety of model-specific histomold designs that enable spatially controlled histological sectioning and downstream analyses. We describe these workflows, including mold generation, high-plex staining, and image analysis, and exemplify their application to histological analyses of various CIVMs. Altogether, the histomolds introduced here afford opportunities for CIVM processing and analysis, while significantly reducing labor and reagent resources, thereby democratizing high-throughput handling of CIVMs in histopathology.

INTRODUCTION

Complex *in vitro* models (CIVMs) have emerged as revolutionary tools to study human physiology.[1–5] These—often patient-derived—three-dimensional (3D) *in vitro* systems generally surpass conventional 2D models, as they more accurately recapitulate the architecture and functionality of the respective organ of origin, therefore opening avenues to understand human tissue function in health and disease.[6–10] Among the most notable models are patient-derived explants,[11–13] organ-on-chip systems,[14–17] barrier tissues grown on transwells,[18–21] as well as organoids,[22–27] which can be subjected to various culture methods and even supplemented with immune or stromal cells to study organ-level processes.[28–32] Due to the diversity of the models, combined with a vast number of permutations in culture techniques, fast and reliable characterization of such lab-grown structures is critical for their integration into basic and translational research.[33–35] Histology has been a cornerstone for primary organ assessment and CIVM characterization for decades, as it provides insight into the cellular composition and spatial

context of the tissue examined. To assess CIVMs with histological readouts, formalin-fixed, paraffin-embedded (FFPE) blocks are typically prepared per individual sample and subsequently sectioned using a microtome, resulting in thin sections of the specimen. Despite the wealth of information that histological readouts offer, it is traditionally a very low-throughput method, characterized by time-consuming, manual workflows that are not well suited to accommodate large sample volumes.[36,37] These drawbacks are particularly pronounced in the case of CIVMs, as they are often very small in size, demand complex culture vessels that complicate the handling and embedding workflows significantly, while yielding low biological material per section.

Recent efforts have aimed to address the aforementioned challenges of embedding organoids for histopathological analysis. Zhang et al.[38] utilized centrifugation to concentrate organoid samples in agarose pellets, whereas others deployed HistoGel to embed organoids directly from culture plates.[39] While these approaches increased the organoid density per section, they did not enhance FFPE embedding throughput, still demanding sample-by-sample processing. Inspired by tissue microarrays,[40–42] some groups have developed negative molds for high-throughput, co-planar embedding of zebrafish and CIVMs.[43–46] However, these workflows require advanced fabrication methods like computer numerical control (CNC) milling and polydimethylsiloxane (PDMS) lithography, which are infeasible to implement in standard histology labs. In addition, current protocols focus on large-sized models (typically >800 μm^3), such as neural or retinal organoids, which are comparably simple to handle.[36,37,46–48] More complex models, such as epithelial monolayers cultured on transwells, organoids grown in an extracellular matrix (ECM), or organoids co-cultured with immune cells, remain unaddressed, highlighting the need for a pragmatic solution to embed these CIVMs into histopathological workflows efficiently.

Here, we present a comprehensive "histo-workflow" to overcome current limitations in CIVM-FFPE processing, data acquisition, and analysis. Our approach is demonstrated across various CIVM types, including organoids cultured in matrix and transwells. This blueprint stands on two pillars: first, 3D-printed "histomolds" to enable straightforward, co-planar, high-throughput embedding of a wide range of CIVMs. Second, an optimized workflow for sample transfer, FFPE embedding, staining, and analysis of dozens of samples within a single section. Beyond that, we provide a protocol for preserving spatial relationships in ECM-embedded cultures, enabling the study of spatially intact epithelial-immune cell interactions. Finally, we validate our workflow with extensive datasets using conventional FFPE staining techniques and provide a feasibility study for spatial transcriptomics.

RESULTS

Histo-workflow for complex *in vitro* systems at high throughput

We describe a blueprint to embed CIVMs in histopathology workflows at high throughput, facilitated by "histomolds." The histomolds were designed and 3D printed to address the embedding requirements of various CIVMs. Crucially, the approach described here does not require any modification of conventional histology workflows (Figures 1A and S1A). Briefly, 3D-printed histomolds contain an array of protrusions of round or rectangular shapes. Their overall size is governed by the dimensions of standard biopsy casettes (32 × 26 mm), metallic molds (32 × 24 mm) for FFPE blocks, and conventional glass slides (75 × 25 mm). After filling the histomolds with liquid HistoGel, the gel is allowed to polymerize, resulting in a countermold comprising an array of wells (Figures 1A and S1A), enabling co-planar embedding of up to 80 samples. Hereafter, we refer to the demolded countermold as "histoarray." Once transferred into the histoarray, the samples are covered with an additional layer of liquid HistoGel to obtain a histoarray that fully encapsulates the samples (Figures 1A and S1B). Afterward, the histoarray is processed using standard procedures to generate FFPE blocks (Figure S1C).

By design, CIVMs can drastically differ from one another due to model-intrinsic and -extrinsic factors. These parameters directly steer the histomold design and histoarray embedding workflow and, hence, demand different protocols per CIVM. To overcome this hurdle, we have designed a range of histomolds to facilitate simple and fast embedding of various CIVMs, while retaining a high density of wells per histomold (Figure S1). We grouped the CIVM landscape into four workflows, aiming to develop overarching protocols governing the most common models and culture protocols in the field.

(1) Single, small- to large-sized models (Figures 1B and 1C, S1D, and Figure S2)
(2) Epithelial monolayers cultured on transwells and hydrogels (Figures 1D and 1E)
(3) Soft ECM and suspension culture models (Figure 1F)
(4) Stiff ECM co-culture models (Figure 1G)

The workflow is agnostic to the biological identity of the sample and is almost exclusively determined by the respective intrinsic and extrinsic factors of the system (features of CIVMs determining histomold design), and hence is applicable to any CIVM (Figures 1B–1G and S1D). Altogether, the high-content nature of the histoarrays significantly reduces manual, labor-intensive procedures while concurrently diminishing the consumption of expensive reagents. To illustrate these points, we showcase CIVMs of each aforementioned group and the respective workflows.

High-throughput embedding of single, large-sized CIVMs

Cultures of animal- or human-derived tissue fragments *ex vivo* (explants) serve as models of the highest compositional complexity, preserving cell populations found *in vivo*, along with their spatial relationships, relative abundances, and native ECM.[49] These models have recently been utilized to study immune cell activation in tumor tissues in response to specific immune checkpoint blockades,[50] chemotherapy,[51,52] targeted therapies,[53,54] exposure to oncolytic viruses,[55] assessment of fibrotic changes,[56] and studies of disease-specific mechanisms.[57] While whole-mount light microscopy enables high-throughput imaging assessment, it remains challenging for large, cellular-dense models, such as explants, due to insufficient light

CellPress
OPEN ACCESS

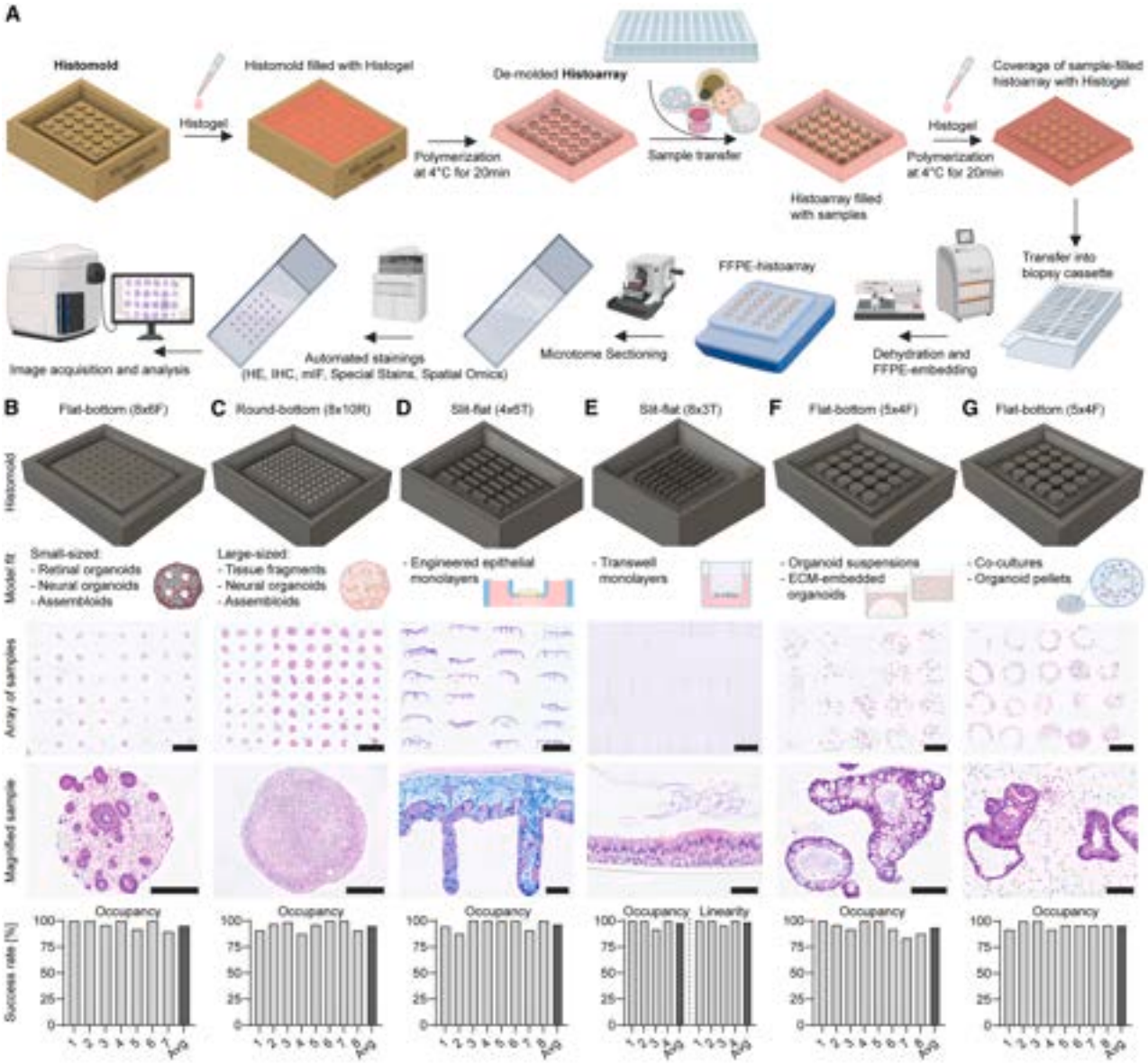

Figure 1. High-throughput histo-workflow facilitated by histomolds for complex *in vitro* systems in histopathology

(A) Illustration of the entire histo-workflow (schematic created in BioRender).

(B–G) Non-exhaustive histomold overview across routinely used *in vitro* models, including histoarray well success rate (including occupancy and linearity), quantified and averaged across multiple CIVMs (n = 4–8). Histoarray overview scale bars, 2.5 mm. (B) Forty-five single, small-sized colorectal cancer assembloids; magnified hematoxylin and eosin (H&E) image highlights a single assembloid (Scale bars, 250 μm). (C) Seventy-eight large-sized mouse neural organoids; magnified H&E image shows a single organoid (scale bars, 250 μm). (D) Twenty-two engineered intestinal epithelia perpendicularly embedded; magnified Alcian Blue/PAS cross-section showcases mucus layer (scale bars, 125 μm). (E) Twenty-four alveolar epithelia perpendicularly embedded; magnified H&E image shows ciliated bronchial epithelium with apically secreted mucus (scale bars, 50 μm). (F) Twenty wells of intestinal organoids; magnified H&E image shows two intestinal organoids (scale bars, 100 μm). (G) Twenty peripheral blood mononuclear cell (PBMC)-intestinal organoid co-cultures; magnified H&E image shows PBMCs within the matrix surrounding intestinal organoids (scale bars, 100 μm).

penetration. This limitation is typically remedied by FFPE-based imaging, albeit at the cost of throughput.

To overcome this, we designed a histomold with appropriate well dimensions typical of explants (8 × 6R histomold, Figure S3), enabling co-planar embedding of 48 samples within a single FFPE block. After 24 h of culture, explants were fixed and individually transferred to a histoarray using tweezers (Figure 2A). Tissue morphology of the explants was assessed by hematoxylin and eosin (H&E) (Figure 2B), which highlighted a systematic lack of organized crypt and villus structures in the tumor explant cohort, while normal explants showed a substantial presence of debris after 24 h in culture (Figure 2B). Multiplex

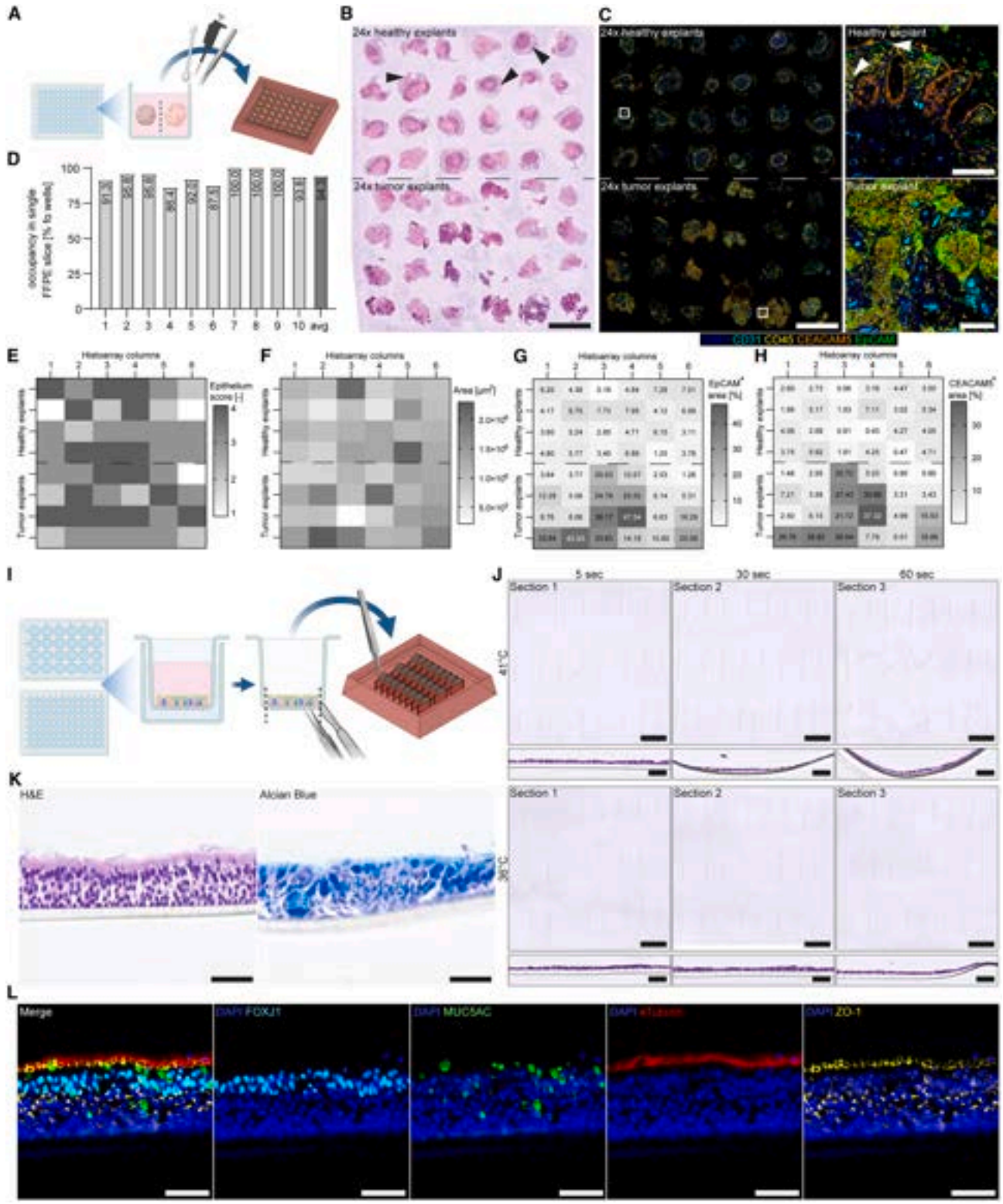

Figure 2. Histo-workflow for single, large-sized and transwell-cultured CIVMs: Analysis of tissue fragments at high-throughput and perpendicular assessment of lung epithelium

(A) Schematic of explant embedding workflow by direct transfer of tissue fragments into an 8 × 6R histoarray. Schematic created in BioRender.

(legend continued on next page)

immunofluorescence (mIF) confirmed a wide heterogeneity in cellularity within the tumor explants, with certain fragments displaying packed and disorganized epithelial regions, while other fragments were composed predominantly of stroma, directly reflecting the organizational heterogeneity characteristic of tumor tissues (Figure 2C).

As explants represent the full range of compositional heterogeneity of the tissue of origin, and, further, due to the manual preparation of fragments and potential residual mucus, explants show a considerable variability in size. Regardless, the described workflow allowed us to achieve an average of 94% occupancy of histoarray positions by explants in sections (Figure 2D).

To assess how robustly the epithelium was represented in the generated explants across three histoarrays (Figure 2E; non-cultured), the ratio of epithelium-positive area to overall tissue fragment size was scored: a score of 1 indicated 0%–25% epithelium-positive area per fragment, 2 indicated 25%–50%, 3 indicated 50%–75%, and 4 indicated explants with 75%–100% epithelial coverage. We determined that the average probability of observing explants with more than 50% of the area positive for epithelium (i.e., a score of 3 or 4) was 79.9% (Figure 2E). Together, these data indicate that the workflow yields explant histoarrays with nearly all wells occupied in any given FFPE section, and each well has a high probability of predominantly exhibiting epithelium.

Next, we utilized the dense sample-array section to quantify expression of targets for immunotherapy,[58] obtaining an overview of the variability in expression among multiple explants sourced from the same baseline tissue, including donor-matched normal and tumor tissue. Specifically, we quantified CEACAM5 and EpCAM expression, followed by quantification of antigen-expressing areas relative to respective cohesive fragment areas (Figures 2F–2H). Explants from tumor and normal tissue showed similar size distributions and, for this tissue donor, tumor explants displayed higher levels of both EpCAM and CEACAM5 compared to normal explants, with both groups showing high variability in antigen expression (Figures 2G and 2H). Collectively, these data showcase the potential of the histoarrays for high-throughput embedding, staining, and analysis of donor-matched healthy and diseased tissue explants, which is directly translatable to other large sized models (Figure S2).

Perpendicular cross-sections facilitated by histoarrays

Transwells are among the most common culture vessels to study lung epithelial barrier integrity,[59] infection,[60] drug delivery,[61] and basic functions of barrier tissues.[62] Specifically, air-liquid interface (ALI) lung transwell systems are well established, as the ALI supports epithelial cell differentiation.[63,64] As these systems require multi-week differentiation protocols to generate a mature epithelium, FFPE-based assessment is particularly valuable, as multiple sections can be obtained for both morphology and marker assessment. However, conventional perpendicular embedding of lung transwells is notoriously difficult and low throughput, as it requires precise placement of the transwell at 90° in the metallic mold while pouring and polymerizing the paraffin to obtain a sufficient cross-section.

To overcome this, we designed histomolds with thin slit protrusions with the dimensions of standard 96-well and 24-well transwells that substantially ease the embedding of transwells (8 × 3T and 3 × 5T, Figure S3). Post-fixation, we removed multiple sample-membrane constructs using either forceps to peel away the membrane (for 96-well transwells), a scalpel, or a biopsy puncher (for 24-well transwells) and transferred them directly to the histoarray, which guides perpendicular embedding by design (Figure 2I). Notably, we identified that water bath temperature and incubation time during sectioning significantly impacted sample integrity and section quality. Short incubation times of 5–10 s reliably yield high-quality H&E sections with straight samples and with the majority of the epithelium in focus on scanned slides, regardless of water bath temperature (Figure 2J). However, longer incubation times using a standard water bath temperature of 41°C result in frequent sample loss and progressive waviness in the sample-membrane constructs, with associated obscuration of the epithelium by the transwell membrane and intermittent regions that are out of focus. In contrast, using a lower water bath temperature of 36°C results in minimal drop-off in section quality with up to 60 s incubation time. Thus, careful control of these variables is critical for enabling higher throughput histologic evaluation of multiple transwells from histoarray FFPE blocks.

To assess a transwell model of bronchial airway epithelium, H&E and Alcian blue staining was performed, highlighting the pseudostratified epithelium rich in goblet cells (Figure 2K). Using a consecutive section for mIF, we further confirmed the zonated

(B) H&E image showcasing a histoarray containing forty-eight colon tissue samples (24 h *ex vivo* culture), comprising patient-matched normal and tumor explants. Black arrows indicate areas of non-cohesive tissue (scale bars, 2.5 mm).
(C) mIF image exemplifying normal and tumor tissue morphologies. White arrows indicate areas of debris visible in normal explants (EpCAM$^+$, green; CEACAM5$^+$, orange; CD45$^+$, yellow; CD31$^+$, cyan; and DAPI$^+$, blue) (overview scale bars, 2.5 mm; magnified organoid scale bars, 100 μm).
(D) Explant histoarray well occupancy, quantified across 10 colon histoarrays.
(E) Well-by-well scoring of epithelial content across fresh colon explant histoarray; $n = 3$). Score of 1 indicated 0%–25% epithelium-positive area per fragment, 2 indicated 25%–50%, 3 indicated 50%–75%, and 4 indicated explants with 75%–100% epithelial coverage.
(F–H) Quantification of explant cohesive tissue area (left) and EpCAM (center) and CEACAM5 (right) expression in matched normal and tumor explants (24 h *ex vivo* culture). EpCAM and CEACAM5 levels were normalized to the tissue area in each fragment.
(I) Schematic overview of embedding lung transwells by peeling away the specimen-polymer complex with forceps (96-well transwells; 8 × 3T) or by removal with a scalpel (24-well transwells; 3 × 5T) and transfer into the histoarray. Schematic created in BioRender.
(J) Consecutive sections of 10-day-old human primary alveolar epithelial cells cultured on transwells in an 8 × 3T histomold (scale bars, 2.5 mm; magnified insert scale bars, 40 μm).
(K) Representative H&E and Alcian blue images of a pseudostratified bronchial epithelium cultured on a transwell for 30 days (scale bars, 50 μm).
(L) Representative mIF image highlighting the zonated, tight (ZO1$^+$, yellow) and differentiated bronchial epithelium, exemplified by secretory cells (MUC5AC$^+$, green) and FOXJ1$^+$ ciliated cells (cyan) with αTubulin$^+$ cilia (red), including DAPI$^+$ nuclei (blue; scale bars, 50 μm).

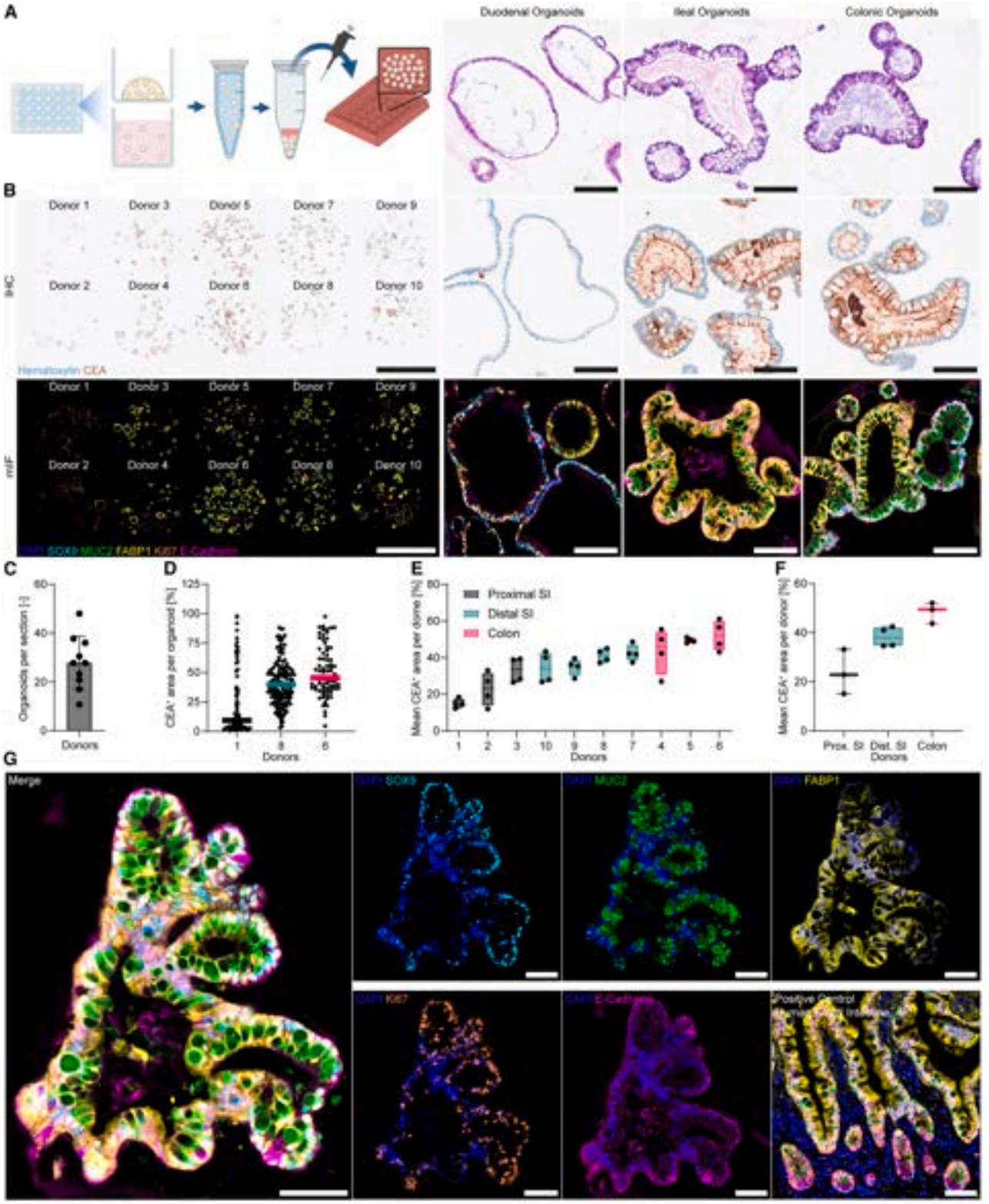

(legend on next page)

architecture, exemplified by FOXJ1^{+} ciliated cells in the top layer of the epithelium, including αTubulin^{+} cilia on top of the polarized epithelium (Figure 2L). Furthermore, strong apical ZO-1^{+} expression highlighted the tight barrier. Goblet cells (MUC5AC^{+}) were mostly found in the upper layer of the epithelium, where they secrete mucus on the apical side of the tissue. This workflow demonstrates the utility of characterizing transwell models, which we recently harnessed to assess the cellular architecture and composition of open-top engineered intestinal epithelia across the ''crypt-villus'' axis[65] (Figure 1D). Additionally, by fully engulfing these *in vitro* intestines with HistoGel in combination with collagen, we have developed a protocol to preserve the intricate secreted mucus in FFPE sections during fixation and dehydration, opening avenues for studying mucus *in vitro*.[65]

High-throughput embedding of soft ECM-embedded and suspension culture models

In the intestine, adult stem cells located at the crypt base give rise to highly specialized, functional epithelial cell lineages, which is mirrored by intestinal organoids *in vitro*.[66] These mini-intestines (adult- or induced pluripotent stem cell [iPSC]-derived) continuously mature in culture, recapitulating aspects of their parent organ. In order to benchmark the status of epithelial differentiation of intestinal organoids, assessment of cell-marker expression is important. However, as intestinal organoids are typically grown in a soft hydrogel (e.g., Matrigel), evaluation of such ECM-embedded systems via histology has proven difficult, primarily due to the challenging retrieval from the matrix.[67]

Here, we demonstrate gentle liberation of soft ECM-cultured organoids by incubating the samples with Cell Recovery Solution for 40 min at 4°C, followed by harvest, fixation, and direct dispensation into the 5 × 4F histoarray (Figures 3A and S3). Utilizing this approach, we were able to co-embed ten intestinal organoid donors in technical duplicates from various intestinal regions (Figure S4A). Using consecutive sections for H&E, immunohistochemistry (IHC), and mIF, we were able to assess morphological integrity by H&E, expression of a cancer immunotherapy-relevant target protein[68–70] (IHC), and heterogeneous organoid differentiation (mIF) from a single FFPE block (Figures 3B, S4B and S4C).

Across the ten different donors, a mean of 28 organoids per section was detected (Figure 3C). Despite this number being sufficient for analysis, the density of organoids per well can be further increased to enhance biological content per section (Figure S4D). Carcinoembryonic antigen (CEA) expression was visualized for all identified organoids of three representative donors (Figure 3D), highlighting the distribution of expression within a technical replica. We then merged the mean of all technical replicas per donor to find that colon organoids have the highest CEA expression level (Figure 3E), reflected by region-specific visualization (Figure 3F). Next, we assessed the heterogeneous differentiation status of the organoids (Figure S4C). While ileal and colonic organoids differentiated well within the culture period, highlighted by ubiquitous FABP1^{+} enterocytes, MUC2^{+} goblet cells and a thick, polarized epithelium (H&E and E-cadherin), such a degree of differentiation was not observed in the duodenal organoids (Figure 3B). As previously reported, intestinal organoids mimic the spatial patterning of their organ of origin *in vitro*.[71] We were able to confirm this by direct comparison to primary duodenum tissue (Figure 3G), including crypt-like buds (FABP1^{-}, Ki67^{+}, SOX9^{+}) and a ''villus-like'' area (FABP1^{+hi}, Ki67^{-}, SOX9^{-}).

To broaden the applicability of the histomolds, we assessed whether our histo-workflow is amenable to sensitive spatial transcriptomics methods. To this end, we subjected a small but dense histoarray (8 wells) with intestinal organoids to multiplexed error-robust fluorescence *in situ* hybridization (MERFISH) for FFPE samples (Figure S4E). We confirmed that mRNA quality after histoarray processing was suitable for spatial transcriptomics (DV_{200} 71%, data not shown). In addition, we were able to detect hundreds of transcripts outlining the epithelium of the intestinal organoids (Figure S4E), albeit transcripts per cell being low, demanding further optimization in the future.

Stiff ECM-embedded co-cultures to retain spatial information

With the rise of immunotherapy for a range of immune-mediated pathophysiologies,[72–74] the concomitant contribution of the tumor microenvironment (TME) and spatial context has become increasingly evident.[75–77] Although organoids represent a powerful tool for disease modeling, they are devoid of important tissue compartments such as the immune system, which is fundamental for modeling immunotherapy outcomes. Recently, multiple groups have started to co-culture immune cells with organoids to

Figure 3. Histo-workflow for soft-ECM embedded and suspension CIVMs: Differentiation assessment and cancer immunotherapy target expression of intestinal organoids

(A) Schematic overview of processing soft ECM-embedded organoids (e.g., Matrigel) by organoid recovery from matrix and/or suspension-cultured organoids, followed by dispensation into a histoarray. Schematic created in BioRender.

(B) Representative H&E, IHC, and mIF images of half of the 5 × 4F histoarray across all donors, including dozens of 6-day-old organoids per well (scale bars, 2.5 mm). Magnified inserts highlight representative organoids from different regions, demonstrating a polarized epithelium (strong apical CEA^{+} expression,brown; E-Cadherin^{+}, pink) with stem cell-associated cells (SOX9^{+}, cyan), goblet cells (MUC2^{+}, green), enterocytes (FABP1^{+}, yellow), proliferating cells (Ki67^{+}, orange), and DAPI^{+} nuclei (blue). Magnified inserts scale bars, 100 μm.

(C) Mean organoid number per section across the ten donors (± SD).

(D) Quantification of CEA^{+} area of all organoids in one histoarray well of three representative donors (n_{orgs}>78 per donor).

(E) Quantification of the mean CEA^{+} expression of organoids per well across two sections per donor (n = 4 per donor). Boxplots with whiskers showing all points (minimum to maximum)

(F) Mean CEA^{+} expression across two sections per donor with respect to the region of origin (n = 3–4). Boxplots with whiskers showing all points (minimum to maximum)

(G) Example of a 6-day ileal intestinal organoid, showcasing differential marker expression between a crypt-like area (Ki67^{+}, SOX9^{+}, and FABP1^{-}) and a villus-like structure (Ki67^{-}, SOX9^{-}, and FABP1^{+}), including parental tissue (scale bars, 100 μm).

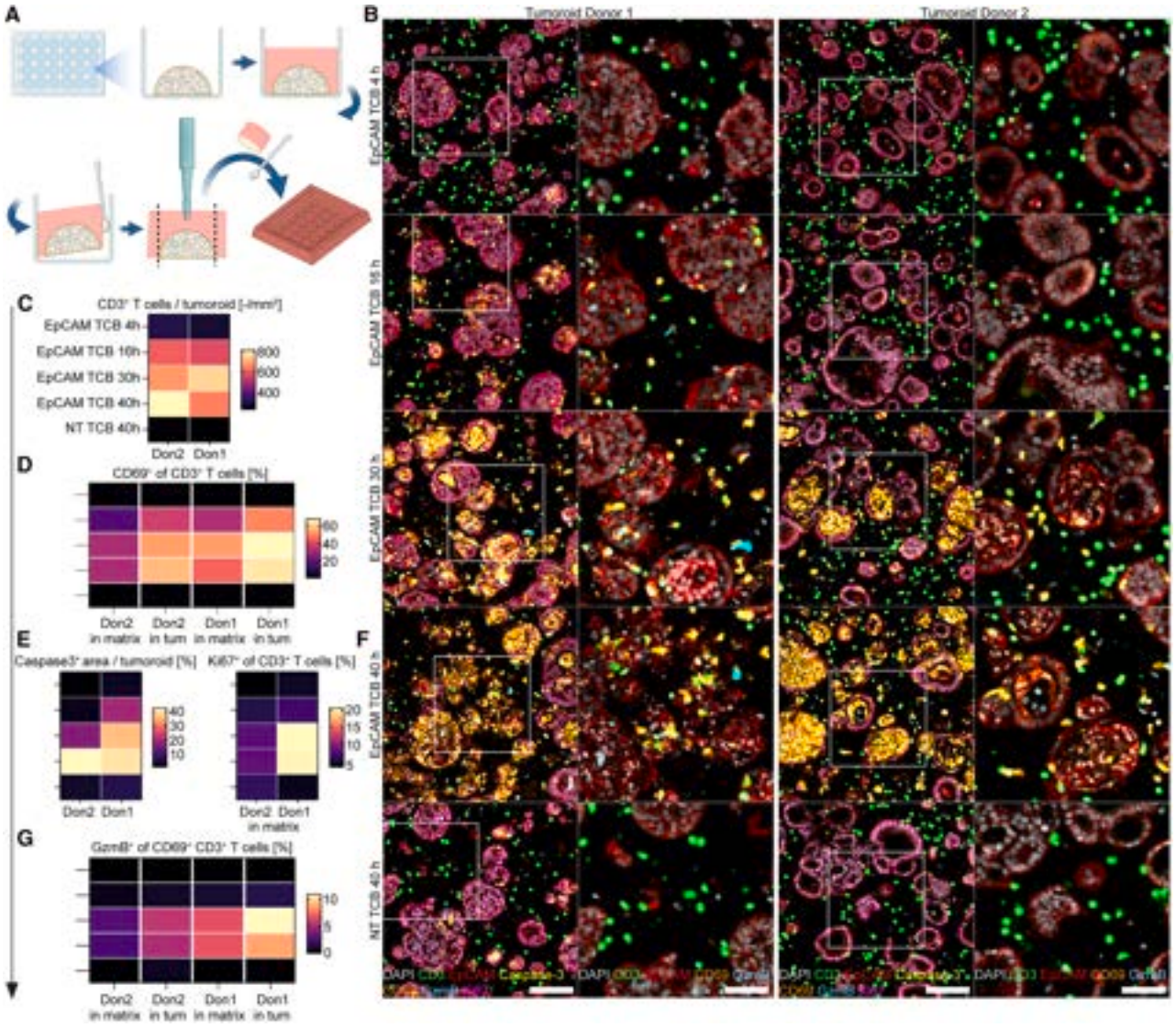

Figure 4. Histo-workflow for stiff-ECM embedded CIVMs: Spatiotemporal analysis of T cell bispecific efficacy assessment on immune-tumoroid co-cultures

(A) Schematic overview of embedding stiff ECM-cultured (e.g., Collagen-Matrigel) PBMC-intestinal tumoroid co-cultures to retain spatial organization by in-well HistoGel polymerization, followed by lifting and punching out the co-culture dome and transfer to the 5 × 4F histoarray. Schematic created in BioRender.

(B) Representative mIF images following activation of T cells and subsequent cytolysis of tumoroids post EpCAM TCB treatment (5 μg/mL) per donor and time point from the same histoarray section (scale bars, 100 μm). Magnified inserts (scale bars, 50 μm).

(C–G) Quantification of EpCAM TCB-triggered $CD3^+$ T cell infiltration (green) per tumoroid ($EpCAM^+$, red), followed by upregulation of the activation marker $CD69^+$ (orange) and cytotoxic granules ($GzmB^+$, cyan), resulting in caspase-3^+ apoptosis (yellow) of the tumor epithelium, induction of $CD3^+$ T cell proliferation (pink), and $DAPI^+$ nuclei (gray) (n = 3–4).

overcome this gap.[78–82] However, these cultures are typically subjected to destructive methods such as flow cytometry, or the soft-ECM (e.g., Matrigel) disintegrates upon fixation, thereby losing spatial context and information about the TME.[83] To overcome this gap, we have recently engineered a stiff collagen-Matrigel matrix that withstands fixation and hence enables the assessment of immune-organoid interactions in the context of the microenvironment (Figure 4A)[84]. Briefly, after fixation of the samples in the well, HistoGel is dispensed and polymerized on top of the dome inside the plate. Afterward, the dome-HistoGel construct can be retrieved, excess HistoGel removed, and the sample transferred to a histomold. By utilizing this protocol to retain spatial integrity of co-cultures with the histomolds, we aimed to assess the spatio-temporal anti-tumor effect of an EpCAM-targeting T cell bispecific (TCB) on peripheral blood mononuclear cell (PBMC)-tumoroid co-cultures within one FFPE block.

To this end, we treated the co-cultures (two tumoroid donors) with 5 μg/mL of EpCAM-TCB across four time points (in

duplicates) and transferred the resulting 20 stiff-ECM domes into a single 5 × 4F histoarray (Figure S3). Deploying a 7-plex mIF approach (Figure S5A), we were able to observe increasing apoptosis induction (caspase-3$^+$ cells) in the tumoroids (EpCAM$^+$) and strong co-expression of CD69 (activation) in CD3$^+$ T cells in a temporal manner across both donors (Figure S5B).

We found that T cells increasingly infiltrate the tumoroids (Figures 4B and S5C), become activated (CD69$^+$ CD3$^+$), upregulate cytotoxic GzmB$^+$ granules, and start to proliferate (Ki67$^+$), leading to the induction of apoptosis (caspase-3$^+$) in the EpCAM$^+$ tumoroids (Figures 4B–4G). Notably, T cells within the tumoroids exhibited higher levels of CD69 and GzmB than those remaining in the matrix, suggesting a TCB-triggered, local response by T cells in close proximity to the antigen, followed by activation of T cells in the periphery (matrix; Figures 4B–4D, 4G and S5C). This highlights the need for evaluating such co-cultures in the context of cancer immunotherapy using spatial methods. Harnessing this approach, we were recently able to capture differential infiltration and killing patterns of T cells in the context of healthy and cancerous epithelium from the same donor.[84] Furthermore, we have utilized this approach to study the intraepithelial character of tissue-resident memory T cells when co-cultured with autologous organoids at homeostasis,[85] opening possibilities to study epithelium-immune interactions *in vitro*.

DISCUSSION

The field of CIVM research is rapidly evolving and opens avenues for basic and translational research. With the legal removal of animal testing as a necessity to advance molecules in pharmaceutical development (FDA Modernization Act 2.0[35]), it has become paramount to incorporate CIVMs at each stage of preclinical development. Therefore, in-depth and systematic characterization of these models is pivotal. As histological data has been part of the standard repertoire for regulatory authorities for decades, it is logical to apply these readouts to CIVMs. However, to facilitate the large sample volumes of the CIVM research field, protocols must be developed to overcome traditionally low-throughput and labor-intensive histopathology workflows.

Here, we developed a holistic histo-workflow for CIVMs that overcomes multiple shortcomings of traditional histo-processing and showcases the great potential of histopathology for CIVMs. In particular, we have generated a large battery of histomolds designed to enable high-throughput embedding of a wide range of CIVMs of various sizes, morphologies, culture vessels, and methods. Our 3D-printed histomolds can be easily designed, manufactured, and adapted, while requiring relatively low expertise and inexpensive equipment. Once routinely applied, the transfer of samples is swift, enabling co-planar embedding of up to 80 samples in one FFPE-block. Determined by the depth of the sample in the histoarray, dozens (e.g., dome co-cultures) to hundreds of consecutive sections (e.g., transwells) can be obtained and stained to interrogate the models. Furthermore, the arrayed layout eases image analysis, as intra- and inter-staining variability is minimized. Additionally, various types of negative controls can be co-embedded by experimental design, further simplifying detection scoring or identification of nonspecific antibody binding. Moreover, we demonstrated that the dense sample array facilitated by the histomolds is ideal to accommodate highly advanced and costly spatial transcriptomics methods such as MERFISH, broadening the applicability of the method.

Limitations of the study

Although the histomolds offer great promise and are generally easy to use and implement, the process of embedding and subsequent sectioning can be challenging, particularly in the case of small, spherical models (<500 μm^3) that are intended to be embedded in individual wells (e.g., 8 × 6R; Figure S3). To overcome this, pooling the specimens by resuspending multiple technical replicates in HistoGel and directly dispensing them into, for example, the 6 × 4F histoarray (Figure S3) will generate a greater sectioning depth and more biological material per well. While pooling defeats the purpose of individual embedding, it is a pragmatic solution for embedding and processing small model systems. Importantly, individual assessment of single objects within pooled samples is not defeated but is achievable through downstream object segmentation in the image analysis pipeline, as demonstrated in Figure S4C. Dehydration errors can be easily avoided by sufficient pre-dehydration in formalin as well as by minimizing the thickness of the histomolds in the design phase, as we found larger volumes of HistoGel to correlate with dehydration issues. Lastly, although the process to generate our histomolds is significantly easier than previous workflows,[43,45,46] it still requires some basic 3D printing knowledge. However, with the 3D-printing templates provided in this manuscript, the histomolds can be directly printed and integrated into any histology-lab routine.

Despite the limitations of this study, the histomolds and data presented here afford opportunities for CIVM processing and analysis, while significantly reducing labor and reagent resources, thereby democratizing high-throughput embedding of CIVMs in histopathology.

RESOURCE AVAILABILITY

Lead contact

Requests for further information and resources should be directed to and will be fulfilled by the lead contact, Nikolche Gjorevski (nikolche.gjorevski@roche.com).

Materials availability

To democratize the widespread use of the histoarrays, we provide all the necessary information for other groups to generate them, assuming the availability of required equipment (e.g., 3D printers). The resources to generate the histomolds (STL and STEP files) can be found here: https://doi.org/10.6084/m9.figshare.31077718.

Data and code availability

- Data reported in this paper will be shared by the lead contact upon request.
- This paper does not report original code.
- Any additional information required to reanalyze data reported in this work is available from the lead contact upon request.

ACKNOWLEDGMENTS

We thank the Pathology Core Labs of pRED, Pathology and Applied Safety Science (PASS), for their general lab support and technical guidance, in particular Christelle Zundel, Luisa Bell, and Nadine Stokar. Additionally, we wish to thank the following individuals and core labs at Genentech: Linda Rangell for project support and guidance; Emily Mu for timely generation of transwell samples to enable optimization of the transwell histomold design; and the Digital Pathology Image Analysis group in Research Pathology for whole slide scanning support. Furthermore, we would like to thank David Suter for sharing the murine embryonic stem cell line SBR. Lastly, we thank Mikhail Nikolaev for the open-top chip illustration.

AUTHOR CONTRIBUTIONS

M.F.H. conceived the study. M.F.H. wrote the manuscript with support from E.D.A., E.R.S., I.P., and N.G. M.F.H., B.L., A.M.F., C.H., and E.R.S. optimized the histo-workflow. C.H. and E.R.S. co-developed and optimized the 96-well histomolds and protocol together with R.H. and L.M.N., with support from I.P. E.K. co-developed the 24-well histomold with I.P., J.A., and M.F.H. B.L. and B.S. accumulated protocols with support from M.F.H. R.O., M.F.H., J.A., I.P., and J.L.G.-C. conceptualized, designed, and optimized the histomolds with support from colleagues. E.D.A., J.A., E.K., J.-S.D., R.L.-S., C.H., A.M.F., G.B., and E.R.S. contributed models and respective data, with support from G.C.

DECLARATION OF INTERESTS

The authors are current employees of Roche or Genentech, and some are Roche stockholders. Hoffmann-La Roche Ldt. has filed for patent protection on the histomold technology (specifically slit-flat histomolds) described herein. M.F.H., R.L.-S, J.A., I.P., and J.L.G.-C. are named as inventors on the histomold patent.

DECLARATION OF GENERATIVE AI AND AI-ASSISTED TECHNOLOGIES IN THE WRITING PROCESS

AI-assisted technologies were used to check spelling and language in the written text. Following their use, the text was thoroughly reviewed and revised as necessary, with full responsibility taken for the content of the publication.

STAR★METHODS

Detailed methods are provided in the online version of this paper and include the following:

- KEY RESOURCES TABLE
- EXPERIMENTAL MODEL AND STUDY PARTICIPANT DETAILS
  - Tissue samples
  - Complex *in vitro* model culture
  - Intestinal tumoroid co-culture
  - Retinal mouse organoids
- METHOD DETAILS
  - Histomold design and manufacturing
  - Sample harvesting and fixation
  - Fixation & harvest method III: Direct (*in situ*) sample fixation
  - Preparation of histoarrays from histomolds
  - Sample transfer into histoarray and post-processing
  - Sample dehydration, paraffin embedding and sectioning
  - Paraffin embedding
  - Microtome sectioning
  - Histology techniques
  - Sample preparation for MERFISH spatial transcriptomics
  - Imaging
- QUANTIFICATION AND STATISTICAL ANALYSIS
  - Image analysis

SUPPLEMENTAL INFORMATION

Supplemental information can be found online at https://doi.org/10.1016/j.crmeth.2026.101419.

Received: July 12, 2025
Revised: December 22, 2025
Accepted: March 27, 2026
Published: April 23, 2026

REFERENCES

1. Tang, X.-Y., Wu, S., Wang, D., Chu, C., Hong, Y., Tao, M., Hu, H., Xu, M., Guo, X., and Liu, Y. (2022). Human organoids in basic research and clinical applications. Signal Transduct. Target. Ther. *7*, 168.
2. Clevers, H. (2016). Modeling Development and Disease with Organoids. Cell *165*, 1586–1597.
3. Zhao, Z., Chen, X., Dowbaj, A.M., Sljukic, A., Bratlie, K., Lin, L., Fong, E.L.S., Balachander, G.M., Chen, Z., Soragni, A., et al. (2022). Organoids. Nat. Rev. Methods Primers *2*, 94.
4. Corrò, C., Novellasdemunt, L., and Li, V.S.W. (2020). A brief history of organoids. Am. J. Physiol. Cell Physiol. *319*, C151–C165.
5. Simian, M., and Bissell, M.J. (2017). Organoids: A historical perspective of thinking in three dimensions. J. Cell Biol. *216*, 31–40.
6. Drost, J., and Clevers, H. (2018). Organoids in cancer research. Nat. Rev. Cancer *18*, 407–418.
7. Fatehullah, A., Tan, S.H., and Barker, N. (2016). Organoids as an in vitro model of human development and disease. Nat. Cell Biol. *18*, 246–254.
8. LeSavage, B.L., Suhar, R.A., Broguiere, N., Lutolf, M.P., and Heilshorn, S.C. (2022). Next-generation cancer organoids. Nat. Mater. *21*, 143–159.
9. Hofer, M., and Lutolf, M.P. (2021). Engineering organoids. Nat. Rev. Mater. *6*, 402–420.
10. Kim, J., Koo, B.-K., and Knoblich, J.A. (2020). Human organoids: model systems for human biology and medicine. Nat. Rev. Mol. Cell Biol. *21*, 571–584.
11. Hughes, D.L., Hughes, A., Soonawalla, Z., Mukherjee, S., and O'Neill, E. (2021). Dynamic Physiological Culture of Ex Vivo Human Tissue: A Systematic Review. Cancers *13*, 2870.
12. Dorrigiv, D., Simeone, K., Communal, L., Kendall-Dupont, J., St-Georges-Robillard, A., Péant, B., Carmona, E., Mes-Masson, A.-M., and Gervais, T. (2021). Microdissected Tissue vs. Tissue Slices—A Comparative Study of Tumor Explant Models Cultured On-Chip and Off-Chip. Cancers *13*, 4208.
13. Voabil, P., de Bruijn, M., Roelofsen, L.M., Hendriks, S.H., Brokamp, S., van den Braber, M., Broeks, A., Sanders, J., Herzig, P., Zippelius, A., et al. (2021). An ex vivo tumor fragment platform to dissect response to PD-1 blockade in cancer. Nat. Med. *27*, 1250–1261.
14. McAleer, C.W., Long, C.J., Elbrecht, D., Sasserath, T., Bridges, L.R., Rumsey, J.W., Martin, C., Schnepper, M., Wang, Y., Schuler, F., et al. (2019). Multi-organ system for the evaluation of efficacy and off-target toxicity of anticancer therapeutics. Sci. Transl. Med. *11*, eaav1386.
15. Vernetti, L., Gough, A., Baetz, N., Blutt, S., Broughman, J.R., Brown, J.A., Foulke-Abel, J., Hasan, N., In, J., Kelly, E., et al. (2017). Functional Coupling of Human Microphysiology Systems: Intestine, Liver, Kidney Proximal Tubule, Blood-Brain Barrier and Skeletal Muscle. Sci. Rep. *7*, 42296.
16. Kim, H.J., Huh, D., Hamilton, G., and Ingber, D.E. (2012). Human gut-on-a-chip inhabited by microbial flora that experiences intestinal peristalsis-like motions and flow. Lab Chip *12*, 2165–2174.
17. Huh, D., Matthews, B.D., Mammoto, A., Montoya-Zavala, M., Hsin, H.Y., and Ingber, D.E. (2010). Reconstituting Organ-Level Lung Functions on a Chip. Science *328*, 1662–1668.
18. Cingolani, E., Alqahtani, S., Sadler, R.C., Prime, D., Stolnik, S., and Bosquillon, C. (2019). In vitro investigation on the impact of airway mucus on

drug dissolution and absorption at the air-epithelium interface in the lungs. Eur. J. Pharm. Biopharm. *141*, 210–220.

19. Stone, N.L., England, T.J., and O'Sullivan, S.E. (2019). A Novel Transwell Blood Brain Barrier Model Using Primary Human Cells. Front. Cell. Neurosci. *13*, 230.
20. Wright, C.W., Li, N., Shaffer, L., Hill, A., Boyer, N., Alves, S.E., Venkataraman, S., Biswas, K., Lieberman, L.A., and Mohammadi, S. (2023). Establishment of a 96-well transwell system using primary human gut organoids to capture multiple quantitative pathway readouts. Sci. Rep. *13*, 16357.
21. Bluhmki, T., Bitzer, S., Gindele, J.A., Schruf, E., Kiechle, T., Webster, M., Schymeinsky, J., Ries, R., Gantner, F., Bischoff, D., et al. (2020). Development of a miniaturized 96-Transwell air–liquid interface human small airway epithelial model. Sci. Rep. *10*, 13022.
22. Dye, B.R., Hill, D.R., Ferguson, M.A.H., Tsai, Y.-H., Nagy, M.S., Dyal, R., Wells, J.M., Mayhew, C.N., Nattiv, R., Klein, O.D., et al. (2015). In vitro generation of human pluripotent stem cell derived lung organoids. eLife *4*, e05098.
23. Mun, S.J., Ryu, J.-S., Lee, M.-O., Son, Y.S., Oh, S.J., Cho, H.-S., Son, M.-Y., Kim, D.-S., Kim, S.J., Yoo, H.J., et al. (2019). Generation of expandable human pluripotent stem cell-derived hepatocyte-like liver organoids. J. Hepatol. *71*, 970–985.
24. Takasato, M., Er, P.X., Chiu, H.S., Maier, B., Baillie, G.J., Ferguson, C., Parton, R.G., Wolvetang, E.J., Roost, M.S., Chuva de Sousa Lopes, S.M., et al. (2015). Kidney organoids from human iPS cells contain multiple lineages and model human nephrogenesis. Nature *526*, 564–568.
25. Sato, T., Stange, D.E., Ferrante, M., Vries, R.G.J., Van Es, J.H., Van den Brink, S., Van Houdt, W.J., Pronk, A., Van Gorp, J., Siersema, P.D., et al. (2011). Long-term Expansion of Epithelial Organoids From Human Colon, Adenoma, Adenocarcinoma, and Barrett's Epithelium. Gastroenterology *141*, 1762–1772.
26. Lancaster, M.A., Renner, M., Martin, C.-A., Wenzel, D., Bicknell, L.S., Hurles, M.E., Homfray, T., Penninger, J.M., Jackson, A.P., and Knoblich, J.A. (2013). Cerebral organoids model human brain development and microcephaly. Nature *501*, 373–379.
27. McCracken, K.W., Catá, E.M., Crawford, C.M., Sinagoga, K.L., Schumacher, M., Rockich, B.E., Tsai, Y.-H., Mayhew, C.N., Spence, J.R., Zavros, Y., et al. (2014). Modelling human development and disease in pluripotent stem-cell-derived gastric organoids. Nature *516*, 400–404.
28. Lindemans, C.A., Calafiore, M., Mertelsmann, A.M., O'Connor, M.H., Dudakov, J.A., Jenq, R.R., Velardi, E., Young, L.F., Smith, O.M., Lawrence, G., et al. (2015). Interleukin-22 promotes intestinal-stem-cell-mediated epithelial regeneration. Nature *528*, 560–564.
29. Schreurs, R.R.C.E., Baumdick, M.E., Sagebiel, A.F., Kaufmann, M., Mokry, M., Klarenbeek, P.L., Schaltenberg, N., Steinert, F.L., van Rijn, J.M., Drewniak, A., et al. (2019). Human Fetal TNF-α-Cytokine-Producing CD4+ Effector Memory T Cells Promote Intestinal Development and Mediate Inflammation Early in Life. Immunity *50*, 462–476.e8.
30. Holokai, L., Chakrabarti, J., Broda, T., Chang, J., Hawkins, J.A., Sundaram, N., Wroblewski, L.E., Peek, R.M., Wang, J., Helmrath, M., et al. (2019). Increased Programmed Death-Ligand 1 is an Early Epithelial Cell Response to Helicobacter pylori Infection. PLoS Pathog. *15*, e1007468.
31. Rogoz, A., Reis, B.S., Karssemeijer, R.A., and Mucida, D. (2015). A 3-D enteroid-based model to study T-cell and epithelial cell interaction. J. Immunol. Methods *421*, 89–95.
32. Tsuruta, S., Kawasaki, T., Machida, M., Iwatsuki, K., Inaba, A., Shibata, S., Shindo, T., Nakabayashi, K., Hakamada, K., Umezawa, A., et al. (2022). Development of Human Gut Organoids With Resident Tissue Macrophages as a Model of Intestinal Immune Responses. Cell. Mol. Gastroenterol. Hepatol. *14*, 726–729.e5.
33. Kang, S., Chen, E.C., Cifuentes, H., Co, J.Y., Cole, G., Graham, J., Hsia, R., Kiyota, T., Klein, J.A., Kroll, K.T., et al. (2024). Complex in vitro models positioned for impact to drug testing in pharma: a review. Biofabrication *16*, 042006.
34. Stokar-Regenscheit, N., Bell, L., Berridge, B., Rudmann, D., Tagle, D., Hargrove-Grimes, P., Schaudien, D., Hahn, K., Kühnlenz, J., Ashton, R.S., et al. (2024). Complex In Vitro Model Characterization for Context of Use in Toxicologic Pathology: Use Cases by Collaborative Teams of Biologists, Bioengineers, and Pathologists. Toxicol. Pathol. *52*, 123–137.
35. Stresser, D.M., Kopec, A.K., Hewitt, P., Hardwick, R.N., Van Vleet, T.R., Mahalingaiah, P.K.S., O'Connell, D., Jenkins, G.J., David, R., Graham, J., et al. (2024). Towards in vitro models for reducing or replacing the use of animals in drug testing. Nat. Biomed. Eng. *8*, 930–935.
36. Olsen, T.R., Mattix, B., Casco, M., Herbst, A., Williams, C., Tarasidis, A., Evans, G., Jenkins, L., McMahan, C.L., Simionescu, D., et al. (2014). Processing cellular spheroids for histological examination. J. Histotechnol. *37*, 138–142.
37. Guyon, J., and Daubon, T. (2023). Histological analysis of invasive glioblastoma organoids embedded in a 3D collagen matrix. STAR Protoc. *4*, 102521.
38. Zhang, S.W., Chen, W., Lu, X.F., Wen, Z., Hu, L., Liu, Y.H., Yang, Z., Xue, L., Su, Q., Yan, L.P., et al. (2021). An efficient and user-friendly method for cytohistological analysis of organoids. J. Tissue Eng. Regen. Med. *15*, 1012–1022.
39. Havnar, C., Holokai, L., Ichikawa, R., Chen, W., Scherl, A., and Shamir, E.R. (2024). HistoGel-based techniques for embedding organoids in paraffin blocks enable high throughput downstream histopathological analyses. J. Histotechnol. *48*, 46–57.
40. Beachley, V.Z., Wolf, M.T., Sadtler, K., Manda, S.S., Jacobs, H., Blatchley, M.R., Bader, J.S., Pandey, A., Pardoll, D., and Elisseeff, J.H. (2015). Tissue matrix arrays for high-throughput screening and systems analysis of cell function. Nat. Methods *12*, 1197–1204.
41. Kononen, J., Bubendorf, L., Kallioniemi, A., Bärlund, M., Schraml, P., Leighton, S., Torhorst, J., Mihatsch, M.J., Sauter, G., and Kallioniemi, O.P. (1998). Tissue microarrays for high-throughput molecular profiling of tumor specimens. Nat. Med. *4*, 844–847.
42. Yan, P., Seelentag, W., Bachmann, A., and Bosman, F.T. (2007). An Agarose Matrix Facilitates Sectioning of Tissue Microarray Blocks. J. Histochem. Cytochem. *55*, 21–24.
43. Thomsen, A.R., Aldrian, C., Bronsert, P., Thomann, Y., Nanko, N., Melin, N., Rücker, G., Follo, M., Grosu, A.L., Niedermann, G., et al. (2017). A deep conical agarose microwell array for adhesion independent three-dimensional cell culture and dynamic volume measurement. Lab Chip *18*, 179–189.
44. Simeone, K., Guay-Lord, R., Lateef, M.A., Péant, B., Kendall-Dupont, J., Orimoto, A.M., Carmona, E., Provencher, D., Saad, F., Gervais, T., et al. (2019). Paraffin-embedding lithography and micro-dissected tissue micro-arrays: tools for biological and pharmacological analysis of ex vivo solid tumors. Lab Chip *19*, 693–705.
45. Kabadi, P.K., Vantangoli, M.M., Rodd, A.L., Leary, E., Madnick, S.J., Morgan, J.R., Kane, A., and Boekelheide, K. (2015). Into the depths: Techniques for in vitro three-dimensional microtissue visualization. Biotechniques *59*, 279–286.
46. Gabriel, J., Brennan, D., Elisseeff, J.H., and Beachley, V. (2019). Microarray Embedding/Sectioning for Parallel Analysis of 3D Cell Spheroids. Sci. Rep. *9*, 16287.
47. Chen, J., Ma, H., Deng, Z., Luo, Q., Gong, H., Long, B., and Li, X. (2023). Cerebral Organoid Arrays for Batch Phenotypic Analysis in Sections and Three Dimensions. Int. J. Mol. Sci. *24*, 13903.
48. Heub, S., Navaee, F., Migliozzi, D., Ledroit, D., Boder-Pasche, S., Goldowsky, J., Vuille-Dit-Bille, E., Hofer, J., Gaiser, C., Revol, V., et al. (2022). Coplanar embedding of multiple 3D cell models in hydrogel towards high-throughput micro-histology. Sci. Rep. *12*, 9991.
49. Powley, I.R., Patel, M., Miles, G., Pringle, H., Howells, L., Thomas, A., Kettleborough, C., Bryans, J., Hammonds, T., MacFarlane, M., et al. (2020). Patient-derived explants (PDEs) as a powerful preclinical platform for anti-cancer drug and biomarker discovery. Br. J. Cancer *122*, 735–744.

50. Karekla, E., Liao, W.-J., Sharp, B., Pugh, J., Reid, H., Quesne, J.L., Moore, D., Pritchard, C., MacFarlane, M., and Pringle, J.H. (2017). Ex Vivo Explant Cultures of Non–Small Cell Lung Carcinoma Enable Evaluation of Primary Tumor Responses to Anticancer Therapy. Cancer Res. *77*, 2029–2039.

51. Gerlach, M.M., Merz, F., Wichmann, G., Kubick, C., Wittekind, C., Lordick, F., Dietz, A., and Bechmann, I. (2014). Slice cultures from head and neck squamous cell carcinoma: a novel test system for drug susceptibility and mechanisms of resistance. Br. J. Cancer *110*, 479–488.

52. Naipal, K.A.T., Verkaik, N.S., Sánchez, H., van Deurzen, C.H.M., den Bakker, M.A., Hoeijmakers, J.H.J., Kanaar, R., Vreeswijk, M.P.G., Jager, A., and van Gent, D.C. (2016). Tumor slice culture system to assess drug response of primary breast cancer. BMC Cancer *16*, 78.

53. Demetriou, C., Abid, N., Butterworth, M., Lezina, L., Sandhu, P., Howells, L., Powley, I.R., Pringle, J.H., Sidat, Z., Qassid, O., et al. (2024). An optimised patient-derived explant platform for breast cancer reflects clinical responses to chemotherapy and antibody-directed therapy. Sci. Rep. *14*, 12833.

54. Gavert, N., Zwang, Y., Weiser, R., Greenberg, O., Halperin, S., Jacobi, O., Mallel, G., Sandler, O., Berger, A.J., Stossel, E., et al. (2022). Ex vivo organotypic cultures for synergistic therapy prioritization identify patient-specific responses to combined MEK and Src inhibition in colorectal cancer. Nat. Cancer *3*, 219–231.

55. Runge, A., Mayr, M., Schwaiger, T., Sprung, S., Chetta, P., Gottfried, T., Dudas, J., Greier, M.C., Glatz, M.C., Haybaeck, J., et al. (2022). Patient-derived head and neck tumor slice cultures: a versatile tool to study oncolytic virus action. Sci. Rep. *12*, 15334.

56. Lang, N.J., Gote-Schniering, J., Porras-Gonzalez, D., Yang, L., De Sadeleer, L.J., Jentzsch, R.C., Shitov, V.A., Zhou, S., Ansari, M., Agami, A., et al. (2023). Ex vivo tissue perturbations coupled to single-cell RNA-seq reveal multilineage cell circuit dynamics in human lung fibrogenesis. Sci. Transl. Med. *15*, eadh0908.

57. Ansari, M.Y., Ahmad, N., Voleti, S., Wase, S.J., Novak, K., and Haqqi, T.M. (2020). Mitochondrial dysfunction triggers a catabolic response in chondrocytes via ROS-mediated activation of the JNK/AP1 pathway. J. Cell Sci. *133*, jcs247353.

58. Martínez-Sabadell, A., Morancho, B., Rius Ruiz, I., Román Alonso, M., Ovejero Romero, P., Escorihuela, M., Chicote, I., Palmer, H.G., Nonell, L., Alemany-Chavarria, M., et al. (2022). The target antigen determines the mechanism of acquired resistance to T cell-based therapies. Cell Rep. *41*, 111430.

59. Baldassi, D., Gabold, B., and Merkel, O. (2021). Air–Liquid Interface Cultures of the Healthy and Diseased Human Respiratory Tract: Promises, Challenges, and Future Directions. Adv. NanoBiomed Res. *1*, 2000111.

60. Swart, A.L., Laventie, B.-J., Sütterlin, R., Junne, T., Lauer, L., Manfredi, P., Jakonia, S., Yu, X., Karagkiozi, E., Okujava, R., and Jenal, U. (2024). Pseudomonas aeruginosa breaches respiratory epithelia through goblet cell invasion in a microtissue model. Nat. Microbiol. *9*, 1725–1737.

61. Lee, R.E., Reidel, B., Nelson, M.R., Macdonald, J.K., Kesimer, M., and Randell, S.H. (2023). Air-Liquid interface cultures to model drug delivery through the mucociliary epithelial barrier. Adv. Drug Deliv. Rev. *198*, 114866.

62. Leach, T., Gandhi, U., Reeves, K.D., Stumpf, K., Okuda, K., Marini, F.C., Walker, S.J., Boucher, R., Chan, J., Cox, L.A., et al. (2023). Development of a novel air–liquid interface airway tissue equivalent model for in vitro respiratory modeling studies. Sci. Rep. *13*, 10137.

63. Gras, D., Petit, A., Charriot, J., Knabe, L., Alagha, K., Gamez, A.S., Garulli, C., Bourdin, A., Chanez, P., Molinari, N., et al. (2017). Epithelial ciliated beating cells essential for ex vivo ALI culture growth. BMC Pulm. Med. *17*, 80.

64. Hiemstra, P.S., Tetley, T.D., and Janes, S.M. (2019). Airway and alveolar epithelial cells in culture. Eur. Respir. J. *54*, 1900742.

65. López-Sandoval, R., Harter, M.F., Yu, Q., Gaspa-Toneu, L., Cubela, I., Kromer, K., Aubert, J., Filip, A.M., Kaltenbach, L., Almato-Bellavista, M., et al. (2025). Modeling host-microbe interactions in immunocompetent engineered human gut tissues. Preprint at bioRxiv. https://doi.org/10.1101/2025.05.02.651468.

66. Sato, T., Vries, R.G., Snippert, H.J., van de Wetering, M., Barker, N., Stange, D.E., van Es, J.H., Abo, A., Kujala, P., Peters, P.J., et al. (2009). Single Lgr5 stem cells build crypt-villus structures in vitro without a mesenchymal niche. Nature *459*, 262–265.

67. Co, J.Y., Klein, J.A., Kang, S., and Homan, K.A. (2023). Suspended hydrogel culture as a method to scale up intestinal organoids. Sci. Rep. *13*, 10412.

68. Bacac, M., Fauti, T., Sam, J., Colombetti, S., Weinzierl, T., Ouaret, D., Bodmer, W., Lehmann, S., Hofer, T., Hosse, R.J., et al. (2016). A Novel Carcinoembryonic Antigen T-Cell Bispecific Antibody (CEA TCB) for the Treatment of Solid Tumors. Clin. Cancer Res. *22*, 3286–3297.

69. Tiernan, J.P., Perry, S.L., Verghese, E.T., West, N.P., Yeluri, S., Jayne, D.G., and Hughes, T.A. (2013). Carcinoembryonic antigen is the preferred biomarker for in vivo colorectal cancer targeting. Br. J. Cancer *108*, 662–667.

70. Campos-da-Paz, M., Dórea, J.G., Galdino, A.S., Lacava, Z.G.M., and Santos, M. de F.M.A. (2018). Carcinoembryonic Antigen (CEA) and Hepatic Metastasis in Colorectal Cancer: Update on Biomarker for Clinical and Biotechnological Approaches. Recent Pat. Biotechnol. *12*, 269–279.

71. Fujii, M., Matano, M., Toshimitsu, K., Takano, A., Mikami, Y., Nishikori, S., Sugimoto, S., and Sato, T. (2018). Human Intestinal Organoids Maintain Self-Renewal Capacity and Cellular Diversity in Niche-Inspired Culture Condition. Cell Stem Cell *23*, 787–793.e6.

72. Zhang, Y., and Zhang, Z. (2020). The history and advances in cancer immunotherapy: understanding the characteristics of tumor-infiltrating immune cells and their therapeutic implications. Cell. Mol. Immunol. *17*, 807–821.

73. Mellman, I., Coukos, G., and Dranoff, G. (2011). Cancer immunotherapy comes of age. Nature *480*, 480–489.

74. Wang, Y., Wang, M., Wu, H., and Xu, R. (2021). Advancing to the era of cancer immunotherapy. Cancer Commun. *41*, 803–829.

75. Wang, Q., Shao, X., Zhang, Y., Zhu, M., Wang, F.X.C., Mu, J., Li, J., Yao, H., and Chen, K. (2023). Role of tumor microenvironment in cancer progression and therapeutic strategy. Cancer Med. *12*, 11149–11165.

76. Arner, E.N., and Rathmell, J.C. (2023). Metabolic programming and immune suppression in the tumor microenvironment. Cancer Cell *41*, 421–433.

77. de Visser, K.E., and Joyce, J.A. (2023). The evolving tumor microenvironment: From cancer initiation to metastatic outgrowth. Cancer Cell *41*, 374–403.

78. Dekkers, J.F., Alieva, M., Cleven, A., Keramati, F., Wezenaar, A.K.L., van Vliet, E.J., Puschhof, J., Brazda, P., Johanna, I., Meringa, A.D., et al. (2023). Uncovering the mode of action of engineered T cells in patient cancer organoids. Nat. Biotechnol. *41*, 60–69.

79. Zhong, Z., Quiñones-Pérez, M., Dai, Z., Juarez, V.M., Bhatia, E., Carlson, C.R., Shah, S.B., Patel, A., Fang, Z., Hu, T., et al. (2024). Human immune organoids to decode B cell response in healthy donors and patients with lymphoma. Nat. Mater. *24*, 297–311.

80. Esposito, A., Agostini, A., Quero, G., Piro, G., Priori, L., Caggiano, A., Scaglione, G., Battaglia, A., Calegari, M.A., Salvatore, L., et al. (2024). Colorectal cancer patients-derived immunity-organoid platform unveils cancer-specific tissue markers associated with immunotherapy resistance. Cell Death Dis. *15*, 878.

81. Zhou, G., Lieshout, R., van Tienderen, G.S., de Ruiter, V., van Royen, M.E., Boor, P.P.C., Magré, L., Desai, J., Köten, K., Kan, Y.Y., et al. (2022). Modelling immune cytotoxicity for cholangiocarcinoma with tumour-derived organoids and effector T cells. Br. J. Cancer *127*, 649–660.

82. Kroll, K.T., Mata, M.M., Homan, K.A., Micallef, V., Carpy, A., Hiratsuka, K., Morizane, R., Moisan, A., Gubler, M., Walz, A.-C., et al. (2023). Immune-infiltrated kidney organoid-on-chip model for assessing T cell bispecific antibodies. Proc. Natl. Acad. Sci. *120*, e2305322120.

83. Walsh, L.A., and Quail, D.F. (2023). Decoding the tumor microenvironment with spatial technologies. Nat. Immunol. *24*, 1982–1993.

84. Harter, M.F., Recaldin, T., Gerard, R., Avignon, B., Bollen, Y., Esposito, C., Guja-Jarosz, K., Kromer, K., Filip, A., Aubert, J., et al. (2024). Analysis of off-tumour toxicities of T-cell-engaging bispecific antibodies via donor-matched intestinal organoids and tumouroids. Nat. Biomed. Eng. *8*, 345–360.

85. Recaldin, T., Steinacher, L., Gjeta, B., Harter, M.F., Adam, L., Kromer, K., Mendes, M.P., Bellavista, M., Nikolaev, M., Lazzaroni, G., et al. (2024). Human organoids with an autologous tissue-resident immune compartment. Nature *633*, 165–173.

86. Lancaster, M.A., and Knoblich, J.A. (2014). Generation of cerebral organoids from human pluripotent stem cells. Nat. Protoc. *9*, 2329–2340.

87. Bai, H., Si, L., Jiang, A., Belgur, C., Zhai, Y., Plebani, R., Oh, C.Y., Rodas, M., Patil, A., Nurani, A., et al. (2022). Mechanical control of innate immune responses against viral infection revealed in a human lung alveolus chip. Nat. Commun. *13*, 1928.

88. Dasgupta, Q., Jiang, A., Wen, A.M., Mannix, R.J., Man, Y., Hall, S., Javorsky, E., and Ingber, D.E. (2023). A human lung alveolus-on-a-chip model of acute radiation-induced lung injury. Nat. Commun. *14*, 6506.

89. Völkner, M., Zschätzsch, M., Rostovskaya, M., Overall, R.W., Busskamp, V., Anastassiadis, K., and Karl, M.O. (2016). Retinal Organoids from Pluripotent Stem Cells Efficiently Recapitulate Retinogenesis. Stem Cell Rep. *6*, 525–538.

90. Hötzel, K.J., Havnar, C.A., Ngu, H.V., Rost, S., Liu, S.D., Rangell, L.K., and Peale, F.V. (2019). Synthetic Antigen Gels as Practical Controls for Standardized and Quantitative Immunohistochemistry. J. Histochem. Cytochem. *67*, 309–334.

STAR★METHODS

KEY RESOURCES TABLE

REAGENT or RESOURCE	SOURCE	IDENTIFIER
Antibodies		
Recombinant SOX9 (1:800)	Abcam	Ab185966; RRID: AB_2728660
FABP1 (1:100)	Life Technologies	PA5-28945; RRID: AB_2546421
MUC2 (1:100)	Life Technologies	MA5-12345; RRID: AB_10975230
Ki67 (1:500)	Invitrogen	14-5698-82; RRID: AB_10854564
CD3 (prediluted)	Ventana	790-4341; RRID: AB_2335978
CD4 (prediluted)	Ventana	790-4423; RRID: AB_2335982
CD8 (prediluted)	Ventana	790-4460; RRID: AB_2335985
CD14 (1:200)	Abcam	ab181470, RRID:AB_2725781
CD20 (1:200)	DAKO	M0755
Recombinant CD103 (1:100)	Abcam	Ab227697; RRID: AB_3665840
Cleaved Caspase-3 (1:100)	Cell Signaling Technology	9661; RRID: AB_2341188
EpCAM (prediluted)	Ventana	760–4383
E-Cadherin (prediluted)	Ventana	760–4497
Granzyme B (1:100)	Abcam	Ab4059; RRID: AB_304251
Vimentin (prediluted)	Ventana	790–2917
CD69 (1:100)	Abcam	ab233396; RRID: AB_2922929
MUC5AC (1:100)	Invitrogen	MA5-12178; RRID: AB_10978001
FOXJ1 (1:100)	Invitrogen	14-9965-82; RRID: AB_1548835
aTubulin (1:100)	Abcam	ab218591
PAX6 (1:50)	DSHB	N/A
Rhodopsin (1:200)	Abcam	Ab5417; RRID: AB_304874
OTX2 (1:200)	Atlas/Sigma	HPA000633; RRID: AB_1079538
CRX (1:200)	Abnova	H00001406-M02; RRID: AB_606098
ZO-1 (1:100)	Invitrogen	33-9100; RRID: AB_2533147
CD31 (1:100)	Dako	M0823
CD45 (prediluted)	Ventana	760-2505; RRID: AB_2335953
CEACAM5 (1:200)	Abcam	ab207718; RRID: AB_3086740
Biological samples		
Human intestinal tissue FFPE blocks	Foundation HTCR, Munich, Germany	HTCR ethics commission approval: no. 025-12
Human intestinal tissue FFPE blocks	Clarunis Basel, Switzerland	Ethics Committee of Basel; EKBB, no. 2019-02118
Human intestinal tissue FFPE blocks	Humanitas Research Hospital (Milan, Italy)	ethics commission Comitato Etico Terrirotiale Lombardia 5 (Ethical approval 3631)
Chemicals, peptides, and recombinant proteins		
Phosphate-Buffered Saline (PBS)	Gibco	10010–056
Paraformaldehyde (PFA)	Thermo Scientific Chemicals	J19943.K2
Advanced DMEM/F12	Thermo Fischer Scientific	12634028
Bovine Serum Albumin (BSA)	Sigma-Aldrich	A8412
Cell Recovery Solution	Corning	354253
Sodium Azide	Sigma-Aldrich	S2002
Histogel	Fisher Scientific	12006679
Puncher of various sizes	pfm medical	48401

(*Continued on next page*)

Continued

REAGENT or RESOURCE	SOURCE	IDENTIFIER
CytoOne Multiwell Plates	Star-Lab	CC7682-7524
10% Formalin	Sigma-Aldrich	HT501320
SuperFrost Ultra Plus Gold Adhesion slides	Fisher Scientific	11976299
TeloCol-6	Advanced BioMatrix	5225
Neutralization Solution For TeloCol-6	Advanced BioMatrix	5229
Collagen Rat Tail Type 1	Advanced BioMatrix	5153-1KIT
Tris-EDTA buffer, pH 7.8	Ventana	#950-227
Discovery Inhibitor	Ventana	#760-4840
Discovery Ab diluent	Ventana	#760-108
OmniMap anti-Rabbit HRP	Ventana	#760-4311
OmniMap anti-Mouse HRP	Ventana	#760-4310
OmniMap anti-Rat HRP	Ventana	#760-4457
Discovery ChromoMap DAB Kit	Ventana	#760-159
Hematoxylin II	Ventana	#790-2208
Bluing Reagent	Ventana	#760-2037
Alcohol	Roche	#CAS64-17-5
Xylol	ACROS Organics	#444240050
Standard histoglue	Pertex	#00811-EX
DISCOVERY Ab Diluent	Ventana	760–108
DISCOVERY Inhibitor	Ventana	760–4840
DISCOVERY Goat Ig Block	Ventana	760–6008
OmniMap anti-Ms HRP	Ventana	760–4310
OmniMap anti-Rb HRP	Ventana	760–4311
OmniMap anti-Goat HRP	Ventana	760–4647
OmniMap anti-Rat HRP	Ventana	760–4457
QD DAPI	Ventana	760–4196
ULTRA LCS	Ventana	650–210
Discovery CC1	Ventana	950–500
ULTRA LCS Buffer	Ventana	950–223
Reaction Buffer Concentrate (10X)	Ventana	950–300
DISCOVERY Wash	Ventana	950–510
Tris-EDTA buffer pH 7.8 (CC1)	Ventana	#950-227
Discovery Inhibitor	Ventana	#760-4840
1X Plus Automation Amplification Diluent	Akoya	#FP1609
ProLong™ Gold Antifade Mountant	Invitrogen	#P36930
Mayer's hemalum solution	Sigma-Aldrich	109249
Critical commercial assays		
Gene imaging kit	Vizgen	10400006
Cell Boundary Staining	Vizgen	10400118
Merscope FFPE Sample Preparation reagents	Vizgen	10400114
Merscope FFPE Slide	Vizgen	10500102
1x Automation Amplification Diluent	Akoya	FP1609
Opal 480 Reagent Pack	Akoya	FP1500001KT
Opal 520 Reagent Pack	Akoya	FP1487001KT
Opal 570 Reagent Pack	Akoya	FP1488001KT
Opal 620 Reagent Pack	Akoya	FP1495001KT
Opal 690 Reagent Pack	Akoya	FP1497001KT

(*Continued on next page*)

Continued

REAGENT or RESOURCE	SOURCE	IDENTIFIER
Opal 780 Reagent Pack	Akoya	FP1501001KT
Experimental models: Cell lines		
Human intestinal organoids derived from human intestinal tissue	Foundation HTCR, Munich, Germany	HTCR ethics commission approval: no. 025-12
Human intestinal explants derived from human intestinal tissue	Clarunis Basel, Switzerland and Humanitas Research Hospital (Milan, Italy)	ethics commission Comitato Etico Terrirotiale Lombardia 5 (Ethical approval 3631)
Murine neural organoids from CGR8_SOX1-eGFP_Brachuary-mCherry 202309 mouse embryonic stem cells	David Suter Lab, EPFL, Switzerland	N/A
Human alveolar epithelial cells	Cell Biologics	Cat# H-6053, Lot# F101517Y72
Murine retinal organoids from CGR8_SOX1-eGFP_Brachuary-mCherry 202309 mouse embryonic stem cells	David Suter Lab, EPFL, Switzerland	N/A
Human bronchial epithelial cells	Lonza	#CC-2540, Lot#18TL346815
Software and algorithms		
HALO	Indica Labs	v3.6.4134.396
HALO AI	Indica Labs	v3.6.4134
Ndp.view2	Hamamatsu	https://www.hamamatsu.com/jp/en/product/life-science-and-medical-systems/digital-slide-scanner/U12388-01.html
Other		
Histomold design files	This paper	https://doi.org/10.6084/m9.figshare.31077718
24 mm × 30 mm disposable nbase mold	Thermo Fischer Scientific	22-363-555
Thumb dressing forceps	Roboz	RS8100; Roboz

EXPERIMENTAL MODEL AND STUDY PARTICIPANT DETAILS

Tissue samples

Human tissues and associated clinical information, along with concurrent data collection and experimental procedures, were obtained from patients undergoing tumor resections within the framework of the non-profit foundation HTCR (Munich, Germany) and at the University Center for Gastrointestinal and Liver Disease (Clarunis; Basel, Switzerland) as well as Humanitas Research Hospital (Milan, Italy), including informed patient consent. The HTCR Foundation's framework received approval from the ethics commission of the Faculty of Medicine in the Ludwig Maximilian University (no. 025-12) and the Bavarian State Medical Association (no. 11142). The framework of the University Center for Gastrointestinal and Liver Disease was approved in accordance with the Helsinki Declaration and reviewed and approved by the ethics committee (Ethics Committee of Basel, EKBB, no. 2019–02118). The framework of the Humanitas Research Hospital received approval from the ethics commission Comitato Etico Terrirotiale Lombardia 5 (Ethical approval 3631).

Complex *in vitro* model culture

Intestinal explants

Patient-derived surgical tissue resections were received the morning after surgery. In order to preserve tissue viability, all tissue processing was carried out on ice with addition of sufficient wash medium (advanced DMEM/F12 + 1:250 Primocin +2% PenStrep), to prevent drying out of tissue during manipulation. As a first step, the abundant mucus layer atop the epithelium was gently scraped off using the dull side of a scalpel blade. Secondly, because a full-thickness surgical resection of colon includes mucosal, submucosal and inner and outer muscular layers, the mucosa and submucosa were resected from the remaining tissue prior to fragmentation into explants, by careful separation using a scalpel. Once the relevant layers were selected, explants were generated by cutting the tissue further in the x and y directions until fragments of 1 mm^3 size were obtained. Explants were stored in wash medium on ice until the desired number of fragments were cut, at which point they were distributed into flat-bottom 96 well plates for 24 h *ex vivo* culture in culture medium (advanced DMEM/F12 + 10% FBS + 1X Glutamax +1:250 Primocin +2% PenStrep) at 5% CO2 and 37°C. At culture endpoint, explants were fixed in 4% PFA directly in the culture plate (refer to 'Fixation & Harvest Method III').

Neural organoids

Mouse neural organoids were derived following an adapted version of Lancaster et al. (Nature Protocols, 2014)[86] using the murine embryonic stem cell (ESC) line SBR.

Alveolar and bronchial transwells

Refer to Swart et al. (Nature Microbiology, 2024)[60] for the detailed protocol of the normal human bronchial transwell culture (Catalog #CC-2540, Lot#18TL346815, Lonza).

Alveolar transwell cultures were established using a protocol adapted from an alveolus lung-chip protocol.[87,88] Briefly, human primary alveolar epithelial cells (HPAEC; Cell Biologics, Cat# H-6053, Lot# F101517Y72) from normal lung tissue were expanded to passage 6 (P6) using SAGM Small Airway Epithelial Cell Growth Medium (Lonza, Cat# CC-3118) per the manufacturer's instructions with modifications. Three days prior to seeding, HPAECs were thawed and expanded to P8 in SAGM complete medium, which consists of SAGM supplemented with 5% heat-inactivated fetal bovine serum (HI-FBS; Sigma, Cat# F4135). HTS 96-well transwells (Corning, Cat# 7369) were coated for 30 min at room temperature with an extracellular matrix mixture containing 0.03 mg/mL fibronectin (Corning, Cat 356008), 0.2 mg/mL collagen type IV (Sigma, Cat# C5533) and 0.005 mg/mL laminin (Sigma, Cat# L6274) in endotoxin-free calcium/magnesium-free phosphate buffered saline (PBS; EMD Millipore, Cat# TMS-012-A), then equilibrated with SAGM complete medium in the basolateral compartment. HPAECs were seeded at 1.25 x 10^5 cells/mL (100 μL) on the apical surface and incubated overnight at 37°C in a 5%, humidified CO_2 incubator. The next day, media in both compartments were replaced with SAGM complete media supplemented with 100 nM dexamethasone, 5 ng/mL keratinocyte growth factor (KGF; ThermoFisher Scientific, Cat# PHG0094), 50 μM cyclic adenosine monophosphate (cAMP; Sigma, Cat# B7880) and 25 μM isobutyl methylxanthine (IBMX; Sigma, Cat# I7018). On Day 3, the apical medium was removed to establish an air-liquid interface and the basolateral medium was switched to DMEM/F-12 (Gibco, Cat# 11320033) with 1% pencillin-streptomycin (Gibco, Cat# 15140122), 1X GlutaMAX (Gibco, Cat# 35050061) and 10% HI-FBS. Medium was refreshed every 3–4 days. At Day 7 post establishment of an air-liquid interface (10 days in culture), cells were washed with PBS and fixed in 4% paraformaldehyde (PFA) for 1 h at room temperature before storage in 70% ethanol for FFPE processing.

Intestinal organoids

Refer to Fuji et al.[71] for the detailed protocol of the human intestinal organoid culture.

Intestinal tumoroid co-culture

Refer to Harter et al. [84] for the detailed protocol of the human intestinal tumoroid, immune and tumoroid-immune co-culture.

Retinal mouse organoids

Refer to Völkner et al. [89] for the detailed protocol of the mouse iPSC-derived retina organoid protocol.

METHOD DETAILS

Histomold design and manufacturing

Features of CIVMs determining histomold design.

Histomold Design Parameters	Examples
Size of Specimen	Small (<500 μm^3) vs. Mid (500–1000 μm^3) vs. Large (>1000 μm^3)
Entities per well	Single organoid vs. Multiple organoids
Culture system	Chip vs. (Plate-) Well vs. Transwell
Culture method	Extracellular matrix vs. Suspension

The mold geometry comprises an array of cylindrical wells with a flat or round bottom sharing the same plane of reference. Surrounding this array, a wall made of the same material (cast gel) allows the pouring of gel over the organoids once they are in place. Filling the mold with gel until the wall height results in a uniform block of gel with a top flat surface.

To obtain this design, the casting mold contains the following features (Figure S1E).

- A thick base of lateral dimensions (A-B) 37-31 mm and a minimum height of (I) 12 mm to obtain enough rigidity to ensure a flat 3D printed mold
- A surrounding wall that will contain the first gel to be subsequently demolded. This wall should have a height of (H) 4 mm,and a thickness of (C) 2 mm at its top. An angle (F) 100 °facilitates the demolding of the gel.
- A groove with respect to the middle surface that will create the wall of the demolded gel. This groove has a depth of (J) 2 mm and is (M) 2 mm wide at the base. As before, an angle of (G) 60° facilitates its demolding.

- A middle flat surface with lateral dimensions (D-E) 27-21 mm and protruding cylinders, cuboids or half disks that will serve to form the wells. The exact well sizes used are described in Figure S3 every specific design. In general, the well diameter ranges from 0.25 to 5 mm, and the height from (K) 0.25 to 1.5 mm. For cylinders, the top can be flat or round. In the latter case the round part is a semisphere of radius equal to cylinder radius. The distance between the top of the cylinder/cuboid/disk and the external wall top should be at least (L) 1 mm, to ensure the integrity of the final molded part.

The three dimensional design of the mold was defined by computer aided design software (Autodesk Fusion 360). We additionally provide in supplementary the 3D file of the designs described in this work (key resources able). The design was imported into a 3D printer-compatible software, in our case, PreForm from Formlabs, and we used a Formlabs 3B+ printer. The bottom surface of the mold base was printed directly on the printer base without supports, to ensure a very flat surface. Both elastic and rigid resins were used, the former allowing an easier demolding but requires thicker features to ensure flatness. Specifically, we used Elastic 50A and High Temp resins from Formlabs. After printing, molds were washed and cured according to manufacturer's guidelines: bath in isopropanol under flow (in Form Wash, Formlabs) and 60°C under UV light for 60 min in a curing station (Form Cure, Formlabs).

Sample harvesting and fixation

Fixation & harvest method I: PFA-based sample harvesting

Suitable for: (Soft) ECM-embedded culture models (e.g. Matrigel, Cultrex).

(1) Carefully aspirate the media from the organoid cultures.
(2) Gently wash the organoid cultures with PBS and discard the PBS.
(3) Add 4% PFA to the organoid domes and incubate at room temperature for 30 min. The hydrogel dome will dissociate in PFA.
(4) Transfer the fixed organoids in PFA into a Falcon tube.
(1) Gently pipette up and down along the side wall of the tube to dissolve any remaining hydrogel in the PFA.
(2) Centrifuge the tube at 250xg for 5 min and carefully discard the supernatant containing PFA.
(3) Wash the sample gently with PBS +1% BSA and centrifuge the tube at 250xg for 5 min. Remove the supernatant.
(4) Repeat the gentle wash with PBS +1% BSA.
(5) Remove the supernatant and gently resuspend the fixed organoid pellets in fresh PBS.
(6) Store at 4°C until embedding.

Fixation & harvest method II: Sample harvesting using cell recovery solution

Suitable for: (Soft) ECM-embedded culture models (e.g. Matrigel, Cultrex).

(1) Carefully aspirate the media from the organoid cultures.
(2) Carefully wash the sample with PBS without disturbing the dome.
(3) Remove the wash buffer and add Cell Recovery Solution.
(4) Place the plate in the fridge at 4°C for a minimum of 40 min.
(5) Once the dome has softened or dissolved, resuspend the organoids in the solution by gentle pipetting. The dome will disintegrate, resulting in an organoid-suspension.
(6) Use Advanced DMEM containing 1% BSA (to avoid organoid sticking to tip and tubes) to harvest organoids from the plate into an Eppendorf tube.
(7) Centrifuge at 200xg for 5 min.
(8) Carefully remove the supernatant, as the pellet is not very stable.
(9) Wash the sample gently with cold PBS containing 1% BSA.
(10) Centrifuge again and remove the supernatant.
(11) Fix the organoids with 4% PFA for 30 min at room temperature.
(12) After fixation, centrifuge the tube at 250xg for 5 min and carefully discard the supernatant containing PFA.
(13) Wash the sample gently with PBS +1% BSA and centrifuge the tube at 300xg for 5 min. Remove the supernatant.
(14) Repeat the gentle wash with PBS +1% BSA.
(15) Remove the supernatant and gently resuspend the fixed organoid pellets in fresh PBS.
(16) Store at 4°C until embedding.

Fixation & harvest method III: Direct (*in situ*) sample fixation

Suitable for: Single, mid-large sized models and tissue, stiff ECM-embedded models (e.g. Collagen), transwell monolayer models.

(1) Carefully aspirate the media from the organoid cultures.
(2) Carefully wash the sample once with PBS without disturbing the sample within the culture vessel.
(3) Fix with 4% PFA overnight at 4°C or for 30–120 min at room temperature, based on the sample size within the culture vessel.
(4) After the fixation, wash the sample three times with PBS. Discard the PBS wash.
(5) Add fresh PBS to the sample.
(6) Store at 4°C until embedding.

Fixation & harvest method IV: Direct sample fixation of small organoids

Suitable for: Small suspension culture models.

(1) Transfer the organoids in media into an Eppendorf tube.
(2) Centrifuge the tube at 300xg for 5 min and carefully aspirate the supernatant.
(3) Gently wash the sample with PBS +1% BSA and centrifuge the tube at 300xg for 5 min. Remove the supernatant.
(4) Fix the sample with 4% PFA for 30 min at room temperature or overnight at 4°C.
(5) Centrifuge the tube at 300xg for 5 min and carefully discard the supernatant containing PFA.
(6) Wash the sample with PBS +1% BSA and centrifuge the tube at 300xg for 5 min. Remove the supernatant.
(7) Repeat the wash with PBS +1% BSA.
(8) Remove the supernatant and gently resuspend the fixed organoid pellets in fresh PBS.
(9) Store at 4°C until embedding.

Preparation of histoarrays from histomolds

(1) Select the appropriate histomold suited to the intrinsic and extrinsic factors described above in conjunction with histomolds available (Figure S3).
(2) Retrieve the HistoGel from the fridge and thaw it in the microwave for approximately 10–20 s until it liquefies.

Note: Place the HistoGel tube with a loosened cap inside a 50 mL Falcon tube with its lid slightly closed to prevent the HistoGel from boiling over. Keep the HistoGel at ~64°C while working to maintain its liquid state.

(3) Fill the histomold with HistoGel by pipetting from the corners first, ensuring that you avoid creating bubbles and that the gel is evenly distributed on the surface. It is important to have the HistoGel filled level on the surface, ensuring a flat surface once cast out of the mold.
(4) Polymerize the HistoGel in the mold for 20 min at 4°C in the fridge.
(5) After polymerization, gently remove the HistoGel from the mold and transfer it to a Petri dish or Parafilm (non-sticky/hydrophobic surface) by using spatulas and squeezing it out.

The resulting, cast-out HistoGel is from here onward referred to as ‘‘histoarray’’ (Figure 1A).

Optional: For added stability during sample transfer, place the trimmed histoarray into 24 mm × 30 mm disposable base mold.

Optional: labeling samples to ease identification of samples during sectioning

Identification of the depth positioning of fixed samples within an FFPE block during FFPE sectioning is important for choosing the best possible FFPE slices for staining. For example, choosing sections too early or too far along during the sectioning process can lead to FFPE sections with suboptimal representation of samples or no biological material on the section. However, identification of appropriate cutting depths can be challenging for a variety of reasons: for explants, which vary slightly in size and buoyant properties (as discussed above), identification of fragments may be challenging due to poor color contrast between wax and pale tissues, or due to fragment sizes much smaller than 1 mm^3, as may be needed when testing numerous conditions from an initially scarce surgical resection or biopsy. This can be equally challenging when dealing with small spheroids or organoids liberated from ECM. It is therefore advisable to improve the contrast between the CIVM being embedded and the surrounding material by staining fixed CIVMs with hematoxylin/eosin solution (Mayer’s hemalum solution), prior to embedding into histomolds, especially when beginning to use the histomolds. Toward this, fixed samples are ideally retained in well plates. A drop, equivalent to approx 5-10 μL solution, is added to each well containing the sample in PBS. Samples are allowed to take up the dye at room temperature for 10–30 min, after which PBS + hematoxylin/eosin are removed from the wells using a small-bore tip (to ensure sample exclusion), washed once in PBS and then added to histomolds as described below. If samples are not in well plates, this process can be carried out on sheets of parafilm. Such pre-staining with hematoxylin/eosin greatly aids the identification of ideal sample planes within the FFPE block, as the coloring is retained all the way through FFPE sectioning. Importantly, this staining does not have repercussions on additional H&E staining, nor on (auto)fluorescence levels in mIF stainings.

Sample transfer into histoarray and post-processing

The histomolds described within this manuscript were specifically designed for certain models, sizes and culture vessels in house. However, this is a non-exhaustive list and a constant, reiterative process of adjusting and optimizing the molds further is needed, as new models (might) demand slightly different sized wells or depths, for example. However, the same histomold often accommodates models of different organs of origins or culture methods and even sizes, depending on the user’s preference. The described embedding approaches can be adjusted to needs or preferences of the users and simply outline a variety of workflows we heuristically grouped into four main approaches covering most CIVMs.

In general, the samples can be handled using spatulas, tweezer, pipette tips, or a puncher depending on the model/application/matrix (see below). It is recommended to embed the samples in an asymmetric layout to easily identify samples post-processing and -sectioning, minimizing the chance of mislabeling, as illustrated in Figure S5D. Furthermore, remove as much excess liquid carried over from the samples as possible before transferring into the histoarray to ensure homogenous dehydration results.

In cases where histomolds are to be filled completely, thereby yielding arrays with no evident orientation, it is further recommended to add an additional marker, in order to be able to unequivocally assign the correct orientation of FFPE sections: After filling and polymerizing the histomold completely, the top right corner of the histomold is cut away (Figure S1A), the mold is placed within the histology cassette and, optionally, an appropriately-sized piece of chicken breast tissue (previously fixed in 4% PFA and stored in PBS+sodium azide at 4°) is added to the HistoGel-free corner. The chicken breast is processed alongside the sample in all subsequent steps. Each FFPE section therefore contains a section of chicken breast, positioned in the top right corner of the CIVM histoarray. Chicken muscle is easily visible in H&E sections; in mIF stainings its autofluorescence can be utilized to orient the array to ease analysis. An alternative orientation control is a synthetic antigen gel made of bovine serum albumin (BSA) and containing pigment.[90] To prepare this type of orientation control, add 100 μL of tissue marking dye (TMD-GN, TBS) to 500 μL of 12.5% BSA in PBS (v/v) in a 1.5 mL Eppendorf tube, vortex the tube, heat at 85°C for 10 min on a Thermomixer (Eppendorf), remove the resulting solidified gel from the tube, and trim it into 2 mm × 2 mm x 5 mm pieces. These gel pieces can be placed directly into the notched, HistoGel-free corner of the histoarray and processed alongside the sample, as described above, or the pieces can be wrapped in biopsy paper, processed separately in a tissue cassette, and incorporated at the time of paraffin embedding. These BSA gels do not come off the slide during antigen retrieval and are readily visualized on H&E sections, IHC, and IF.

Transfer method I: Single, mid-large sized models and tissues

(1) Remove the remaining liquid in the culture (Figure 2A) vessel and transfer the fixed sample onto parafilm using spatulas, tweezers or cut-off P1000 tips.
(2) Aspirate any excess liquid carried over.
(3) Place the samples into the histoarray using spatulas, tweezers or pieces of parafilm.
(4) Repeat the previous step in case multiple samples are at hand.
(5) Continue with step A below.

Transfer method II: Epithelial monolayer models on 24-well transwells

(1) Remove the fixed transwell (Figure 2I) samples from the plate.
(2) Either use a scalpel or a biopsy puncher to remove the sample from the transwell insert, including the membrane.
(3) Briefly place the transwell on parafilm (with the polymer facing downward) before transferring it into the histoarray.

Note: do not push the transwell sample into the well, as this might lead to artifacts (e.g., rolling of the specimen at the bottom leading to undesired artifacts).

(4) Repeat the previous step in case multiple samples are at hand.
(5) Continue with step A below.

Transfer method II: Epithelial monolayer models on 96-well transwells

(1) Remove the fixed transwell (Figure 2I) samples from the plate.
(2) Using forceps, grasp the edge of each transwell insert to peel off the sample with the transwell membrane.
(3) Transfer the transwell directly into the histoarray.
(4) Repeat the previous step for all samples.
(5) Continue with step A below.

Transfer method III: Soft ECM-embedded culture models and small suspension culture models

(1) Aspirate liquid in the Eppendorf (Figure 3A) tubes containing the fixed samples to ensure a dry organoid pellet (if necessary, centrifuge one more time).
(2) Resuspend the samples with liquefied HistoGel.

Note: the volume depends on the well size of the intended mold and amount of mold-wells you intend to fill with your samples. Ideally, the denser the better to enable a higher number of biological material per section.

(3) Dispense organoid-HistoGel suspension directly into the wells of the histoarray.
(4) Repeat the previous step in case multiple samples are at hand.
(5) Continue with step A below.

Transfer method IV: Stiff ECM-embedded (co-) culture models

Stiff, collagen-based ECM preparation: To enable handling and embedding of samples without perturbing the spatial integrity (Figure 4A), a stiff ECM is crucial. Recently, we've shown that a Rat Collagen I mixture with Matrigel (1:1 ratio, v/v) mixture is sufficient to retain the spatial integrity of the sample upon PFA fixation and transfer into the histoarray.[84,85] Besides the Rat Collagen I, we have also used Bovine Collagen (Telo-Col 6) with its commercially available neutralization solution that can be used to retain the integrity of the matrix (100% or mixed with Matrigel). Briefly, the stiff ECM was prepared following manufacturers ratios by resuspending 350 μL Telo-Col 6 with 40 μL of Neutralization Solution and mixed thoroughly (alternatively vortexed shortly). Next, the neutralized collagen was thoroughly mixed with 100 μL of Matrigel before centrifuging it for 30 s at 20000 g at 4°C to avoid bubble formation.

Afterward, samples can be resuspended with this hydrogel mixture and dispensed into a 24-well plate.

Note: The more hydrophobic the plate, the smoother the workflow described below (e.g., CytoOne CC7682-7524) as the dome will detach more easily. In addition, as different plates might lead to different sizes of domes (in respect to the total volume of the dome),

the size of the dome (diameter) should be assessed once. The choice of puncher size and histomold-well diameter depends on this.

(1) Remove any liquid from the wells containing the fixed samples.
(2) Add 400 μL of HistoGel to the sample-containing wells, submerging the sample fully.
(3) Place the plate for a minimum of 25 min in the 4°C fridge to ensure full polymerization.
(4) Afterward, use a bent spatula and carefully scoop out the HistoGel-disk containing your sample and place it on parafilm.
    (i) Note: It can happen that the dome does not detach from the bottom of the plate with the HistoGel-disk. However, due to its rigid ECM, it can alternatively be directly removed from the plate using a spatula.
(5) Use a puncher with the appropriate diameter for your dome size and histomold.
(6) Punch the dome out of the HistoGel card and discard the excess HistoGel.
(7) Use two spatulas or parafilm pieces in order to transfer the dome into the histoarray.

Note: The diameter of the puncher and histomold-wells should be exactly the same as this facilitates perfect placement of the samples. For example, the cultures in Figure 4 were cultured in 10 μL matrix. The size of the dome was measured, the histomold wells specifically designed to accommodate the dome (max. 4.1 mm) and a 4 mm puncher selected to retrieve the samples and perfectly place them into the wells of the 5 × 4F flat bottom histomold (Figure S3).

(8) Repeat steps 5–8 in case multiple samples are at hand.
(9) Continue with step A below.

From here, the following steps are applicable to all transfer-workflows described above.

A. Allow the samples to dry in the histoarray for 2 min. Removing excess liquid via pipetting aids the process.
B. Critical: Before completely filling with histoarray, ‘‘glue’’ the samples onto the histoarray by slowly dispensing a few microliters of HistoGel around each sample using a P10 pipette. Wait 5 min to allow for polymerization of the HistoGel.

Note: Filling HistoGel directly on top may cause the samples to lift from the histoarray wells (buoyancy), especially in the case of small/light samples. Carefully pre-polymerizing the samples within the wells before filling the rest of the histoarray prevents this.
Note: Not necessary for ‘Soft-embedded culture models’, which are dispensed in HistoGel directly into the histoarray (see above).

C. Slowly fill up the rest of the mold with HistoGel, keeping it level.
    a. Note: for 96-well transwell samples, add just enough HistoGel to stabilize the samples and prevent them from folding over. Adding a large volume of HistoGel to fully encapsulate the samples will increase the thickness of the histoarray and could increase the risk of distortion artifacts during processing.
D. Place the HistoGel-covered histoarrays in the 4°C fridge for 10-15 min to polymerize the HistoGel.
E. Store any remaining HistoGel at 4°C.
F. Once the HistoGel is polymerized, trim the excess corners of the samples embedded in HistoGel if needed, without disturbing the lanes containing samples, to fit them in the cassette.
G. Place the sample-embedded histoarray inside a histo-cassette without flipping the histoarray.

Critical*:* As the true flat surface is the bottom of the cast histoarray and therefore enables sectioning through all samples at once, the histoarray containing the samples should not be flipped around during the FFPE-embedding process.
Note: It can help to cut a corner of the histoarray in order to identify the orientation later more easily.

H. Place the cassette in 10% formalin for 4 h at RT and proceed with sample dehydration and paraffin embedding afterward.

Note: Store thick Transwell histoarrays for 24 h in 10% formalin at RT followed by 24 h in 70% ethanol to help reduce processing artifacts.

Sample dehydration, paraffin embedding and sectioning

The sample processing is performed in a fully automated tissue processor HistoCore PEARL (Leica).

(1) Place the basket with cassettes in the chamber, select the appropriate program (see below), and start the machine.
(2) Different types of sample blocks require different processing lengths depending on their size or thickness. Refer to the table below for examples. We recommend longer dehydration times for thicker blocks.
(3) The processing retort is initially filled with reagent from the first reaction bottle.
(4) After the set time, the reagent is returned to its respective bottle, and the processing retort is filled with reagent from the next bottle. This process continues sequentially.
(5) Thirteen reagents are exchanged in one cycle within the processing retort.
(6) After the processing cycle is complete, remove the cassette basket and proceed with embedding.

Specified Programs for Processing HistoGel Blocks in the HistoCore PEARL Tissue Processor.

	Normal HistoGel™	Thick HistoGel™
Suitable for:	Histoarray block <0.5 cm thickness	Histoarray block >0.5 cm thickness
	35°C/mix off	35°C/mix off
Formalin	0:05 (delay start)	1:00 (delay start)
EtOH 70%	0:30	1:00
EtOH 70%	0:30	1:30
EtOH 80%	1:00	1:00
EtOH 96%	0:30	1:00
EtOH 96%	0:30	1:30
EtOH 100%	1:00	1:00
EtOH 100%	1:00	1:30
Xylenes	0:45	1:00
Xylenes	0:45	1:30
Paraffin	0:45/56°C	1:00/60°C
Paraffin	0:45/56°C	1:00/60°C
Paraffin	0:45/56°C	1:30/60°C

*To further improve the dehydration procedure, consider using FLEX reagents as an alternative to the ethanol dilution series.

Paraffin embedding

Embedding was performed on a Medite Embedding station TES99.

(1) Take an appropriate metallic-mold and fill half of it.
(2) Open the cassette containing the processed histoarray. Carefully transfer the histoarray from the cassette to the metallic mold filled with paraffin.

Critical: As described above, do not flip the histoarray as the bottom side is intended to be on the bottom of the metallic mold to ensure correct orientation for subsequent sectioning.

(3) Transfer the metallic mold containing the processed histoarray to the cold section of the plate. Gently press the histoarray to the bottom of the mold with tweezers.

Critical: Make sure to equally apply pressure, ensuring the bottom of the histoarray is in one plane.

(4) Cover the mold with the corresponding cassette and fill it with liquid paraffin up to the edge of the cassette. Place it on the cold plate until properly solidified.
(5) After cooling, separate the paraffin block from the mold, remove any excess paraffin, and proceed with sectioning.

Microtome sectioning

Sectioning was performed on a Thermo Microm HM355S.

(1) Fill the water bath with distilled water and adjust the temperature to 42°C.
(2) Trim FFPE-blocks at a thickness of 10–20 μm at room temperature until the first samples appear, then place the FFPE-blocks on a cold plate or an ice bath for 10–15 min, which hydrates and cools the blocks, allowing for better ribbon formation.

Note: The HistoGel has a distinct appearance in contrast to the paraffin, as do the CIVMs in the sections. A trained person will detect even small organoids by eye with ease, whereas non-trained personnel could use the optional labeling step to identify the models during sectioning (described above).

(3) Once the FFPE-blocks are sufficiently cold, section the FFPE-blocks at a thickness of 3–4 μm or thicker sections, depending on the method or requirement. The sections should meet the following criteria:
   (i) All embedded samples must be captured in one plane.Note: If all tips above have been followed, this should be the case.
   (ii) The section must cover the largest surface area of the embedded tissue.Note: Once all samples are captured in one section, perform several consecutive sections at different depths in order to evaluate the section-depth (by H&E, see below).
   (iii) The section must not be wrinkled or folded, this might lead to unwanted artifacts during imaging.

(4) Cut serial sections of 6–7 sections per piece and place them on the surface of the water bath.

Critical: For transwell histoarrays, we recommend setting the water bath temperature to 36°C and collecting only 1-2 sections at a time, optimally within 5–10 s for best results. Flotation times of up to 60 s can be used with relatively minor drop off in section quality. However, if using a standard water bath temperature (41°C–42°C), flotation times longer than 5–10 s result in significant sample waviness and increased sample loss. If a ribbon of serial sections is needed, collect the appropriate number of sections onto the microtome blade holder and transfer to a water bath in smaller ribbons of 2-3 sections.

Note: Separate individual sections using forceps cooled on an ice bath to prevent the transwell samples within the paraffin section from becoming stretched.

(5) Transfer the sections from the water bath onto Superfrost or Gold Superfrost slides.

Note: Use Gold Superfrost slides for thin, long samples (e.g., transwells) to avoid lifting during processing.

(6) After sectioning, place the slides in an incubator at 37°C overnight.
(7) The slides can be stored at room temperature for up to one year.

Depending on the CIVM, we have a two-way sectioning approach.

(a) In case of large samples (e.g., explants or assembloids), we recommend obtaining sections at multiple depths to cover the heterogeneity of the sample.
(b) In case of small samples (e.g., small organoid domes, small kidney organoids), we recommend obtaining as many consecutive sections as possible without trimming at different depths or re-trimming when intending to section the FFPE-block another day to avoid sample loss.

Histology techniques

Hematoxylin and eosin (H&E) staining

H&E staining was executed in a fully automated manner following the standard protocol on the Ventana HE600 stainer (Roche Tissue Diagnostics). H&E stainings were assessed with the ndp.view2 software (Hamamatsu).

Alcian blue staining

Alcian Blue (5279194001, Ventana) -PAS staining (5279291001, Ventana) was performed fully automated on the Ventana Benchmark (Roche Tissue Diagnostics). Briefly, after three cycles of deparaffinization, slides were washed and 200 μL of PAS Alcian blue incubated for 16 min at 37°C. Wash was repeated, and 200 μL of Pas periodic acid was applied for 4 min, before another wash and 12 min of PAS Schiffs staining. Next, slides were washed again and 200 μL PAS neutralizer was added and incubated for 4 min. Lastly, slides were washed with 100 μL before counterstaining the slide with 200 μL of PAS hematoxylin for 8 min. Afterward, slides were coverslipped as indicated in the manufacturer's instructions.

Immunohistochemistry (IHC)

Stainings were performed using Ventana Discovery Ultra automated tissue stainer (Roche Tissue Diagnostics, Tucson AZ USA). Primary antibodies and concentrations were validated in establishment IHC runs (except for pre-diluted Ventana primary antibodies), prepared in Discovery Ab diluent and then subjected to a dispenser for automated application. Specific incubation times might change between antibodies.

(1) Bake the slides first at 60°C for 8 min and subsequently further heat up to 69°C for 8 min for subsequent deparaffinization. Repeat this cycle three times.
(2) Perform heat-induced antigen retrieval with Tris-EDTA buffer pH 7.8 at 95°C for a total of 40 min.
(3) Apply Discovery Goat Ig Block and incubate for 32 min.
(4) Apply Discovery Inhibitor for 16 min.
(5) Apply primary antibodies for 40 min.
(6) Detect primary antibodies using anti-species secondary antibodies conjugated to horseradish peroxidase (HRP) for 16 min and subsequently visualize by conversion of 3,3′-Diaminobenzidine (DAB).
(7) Counterstain specimens with Hematoxylin and Bluing Reagent.
(8) Dehydrate with a standard series of alcohol (70% v/v, 96% v/v, 100% v/v, 100% v/v) and Xylol baths (100% v/v), then mount slides fully automated using the RCM7000 coverslipper and a standard histoglue.
(9) Dry the slides for at least 2 h prior to imaging.

Multiplexed Immunofluorescence (mIF; opal dyes)

Prepare Opal dyes as described by the manufacturer instructions. Stainings were performed using Ventana Discovery ultra automated tissue stainer (Roche Tissue Diagnostics, Tucson AZ USA). Primary antibodies and concentrations were validated in establishment IHC runs (except for pre-diluted Ventana primary antibodies), prepared in Discovery Ab diluent and then subjected to a dispenser for automated application. The order of the primary antibodies and corresponding dyes was further determined during establishment runs. Specific incubation times might change between antibodies.

(1) Bake the slides first at 60°C for 8 min and subsequently further heat up to 69°C for 8 min for subsequent deparaffinization. Repeat this cycle three times.
(2) Perform heat-induced antigen retrieval with Tris-EDTA buffer pH 7.8 at 95°C for a total of 40 min.
(3) Apply Discovery Goat Ig Block and incubate for 32 min.
(4) Apply Discovery Inhibitor for 16 min.
(5) Apply primary antibodies for 40 min.
(6) Apply the respective anti-species secondary antibodies conjugated to horseradish peroxidase (HRP) for 16 min.
(7) Subsequently, apply respective Opal dye (starting with 480–780) and incubate each for 12 min at 37°C, respectively.
(8) After every application of a primary antibody, respective secondary antibody and Opal dye, an antibody neutralization and denaturation step (4 min at 92°C) is applied to remove residual antibodies and HRP, before starting the staining cycle again with the Discovery Inhibitor blocking step (Step 4).
(9) In the seven sequence, after the primary an additional Goat IgG blocking step is performed for 16 min, followed by the secondary antibody-HRP. Next, Opal TSA reagent is applied, followed by the Opal dye 780.
(10) Slides are manually mounted using ProLong Gold Antifade Mountant. Slides are dried for at least 2 h prior to imaging.

Sample preparation for MERFISH spatial transcriptomics

Histomold embedding

Human intestinal organoids growing in domes were washed with PBS and directly fixed with 4% PFA in nuclease-free PBS for 30 min at 4°C. After fixation, the organoids were carefully resuspended by pipetting, transferred to a 50 mL Falcon tube and spun at 300g, 4°C for 4 min. The pellet was washed once with cold nuclease-free PBS with 1% BSA, resuspended in cold nuclease-free PBS with 1% BSA, transferred in a 2 mL tube and spun at 300g, 4°C for 4 min. For embedding, the supernatant was removed and the organoids were transferred into 8 wells of a flat-bottom (5 × 4F) histomold. After drying for ∼2–3 min, a small drop of HistoGel was added on top of each well. After ∼1 min, the gel was filled up and allowed to solidify at 4°C for a few minutes. The HistoGel was placed in a histology cassette and fixed with 10% formalin (HT501320, Sigma) for 1h at 4°C. The cassette was transferred into cold nuclease-free PBS until dehydration and paraffin embedding.

RNA isolation and DV_{200}

The FFPE block was sectioned with a Microtome under RNAse-free conditions. Two sections of 10 μm were deparaffinized with the Deparaffinization solution (19093, Qiagen) and used for RNA isolation with the Qiagen RNeasy FFPE kit (73504, Qiagen). DV_{200} was obtained by running the isolated RNA on an Agilent RNA 6000 Pico Kit (5067-1513) in the Agilent 2100 Bioanalyzer.

MERFISH spatial transcriptomics

The FFPE block was sectioned with a Microtome in RNAse-free conditions. A 4 μm section was placed on a Merscope FFPE Slide (10500102, Vizgen) and processed for MERFISH with Merscope FFPE Sample Preparation reagents (10400114, Vizgen) and user guide Formalin-Fixed Paraffin-Embedded Tissue Sample Preparation 91600112 Rev C (Vizgen). After anchoring pretreatment, the sample was stained with Cell Boundary Staining (10400118, Vizgen) followed by RNA anchoring and gel embedding. The sample was treated with Digestion Mix for 2h at 37°C before undergoing clearing for 24h at 47°C, autofluorescence quenching and further clearing for 24h at 37°C. A custom panel with 409 probes against duodenal cell marker genes was hybridized for ∼46h at 37°C. The slide was washed and imaged on the Merscope instrument (10000001, Vizgen) with a gene imaging kit (10400006, Vizgen) according to Vizgen user guide 91600001. Images were taken with Merscope Vizualizer software.

Imaging

IHC, H&E, and special stains

HE, IHC and special stained slides were imaged with a brightfield whole-slide scanner at 40X (Hamamatsu, NanoZoomer S360).

mIF with Opal kits

Imaging with Vectra Polaris.

(1) Digitize mIF stainings using the Opal dyes from Akoya with multispectral imaging by the Vectra Polaris (PerkinElmer) using the MOTiF technology at 20× magnification for all 7 colors (Opal 480, Opal 520, Opal 570, Opal 620, Opal 690 and Opal 780).
(2) Adjust the laser exposure and intensity settings on multiple slides per staining panel. Scan the slides in a batch manner to ensure same imaging settings and cross-comparability for later image analysis with the image analysis software of choice.
(3) Next, perform unmixing of the channels and tiling of the images with PhenoChart (v1.0.12) and inForm (v2.4).
(4) The raw images were saved as.qptiff and later fused in HALO (Indica labs, v3.6.4134.396).

QUANTIFICATION AND STATISTICAL ANALYSIS

Image analysis

Image analysis of IHC and mIF images was performed with HALO (Indica Labs, v3.6.4134.396) and HALO AI (Indica Labs, v3.6.4134). Sample annotation was swiftly performed using the TMA module in HALO depending on the histomold utilized.

For single organoid detection and annotation (for both IHC and mIF images), a RandomForest (v2) classifier was used to distinguish organoids from background (e.g., matrix; minimum object size >1000 μm). Following manual validation, organoids were handled as individual regions of interest (ROIs) and cell quantification executed per ROI. The RandomForest (v2) classifier was integrated in the Area Quantification (v2.4.3) and Area Quantification FL (v.2.3.4) modules and used to quantify positive marker staining against either overall size of each individual object or normalized to the $DAPI^+$ area of the object (as indicated in legend texts). The HighPlex FL (v4.2.14) module was used to perform nuclear segmentation based on $DAPI^+$ cells, assisted by HALO AI's integrated 'AI default nuclear segmentation type'). Specific cell phenotypes were determined by co-localization of markers of interest with the $DAPI^+$ nuclei (taking the cytoplasm radius (1.25 μm) and nuclear signals into account, respectively). By integrating the RandomForest classifier in the HighPlex module, e.g., localization of the T cells in the matrix or epithelium were determined and normalized to the tumoroid area. Secondary-only staining controls on a consecutive section or primary tissue served as a negative signal threshold to prevent biased adjustments. For some samples, negative controls were co-embedded within the same histoarray to ease unbiased threshold adjustment. For the analysis of antigen-expressing areas in explants, Area Quantification FL (v.2.3.4) was utilized to set the threshold for signal above background for EpCam and Ceacam5 stainings, in order to quantify the area of positivity relative to the area of cohesive explant tissue. Note that for explants generating substantial amounts of debris and loss of tissue cohesion during culture (such as explants generated from normal colon), DAPI signal was used to identify areas of cellular cohesive explant tissue, which were defined with manual ROIs. This effectively removed areas of debris and allowed for more accurate antigen quantification.